Instituto Tecnológico y de Estudios Superiores de Occidente

Reconocimiento de validez oficial de estudios de nivel superior según acuerdo secretarial 15018, publicado en el Diario Oficial de la Federación del 29 de noviembre de 1976.

Departamento de Electrónica, Sistemas e Informática
Maestría en Diseño Electrónico

MITIGATING IMPEDANCE MATCHING DISTURBANCES OF A LONG-RANGE WIRELESS TRANSCEIVER WITH CLASSICAL OPTIMIZATION METHODS

TRABAJO RECEPCIONAL que para obtener el **GRADO** de
MAESTRA EN DISEÑO ELECTRÓNICO

Presenta: **NATALIA CORIA PÉREZ**
Director **DR. J. RAFAEL DEL REY ACUÑA**

Tlaquepaque, Jalisco. 1 de diciembre de 2021.

Summary

This study details the design of a filter and an impedance-matching network for a long-range wireless System on Chip (SoC) by following a methodology based on load-pull analysis results from a well-known supplier to reduce losses and obtain maximum RF performance. The resulting design parameters are used to get optimizable responses to reduce the transceiver RF network's reflection coefficient and loss imbalance. These responses were compared with classical optimization methods applying general gradient-based algorithms and the available downhill simplex Nelder-Mead.

The structure of this essay begins by presenting the basic concepts applied at the foundation of this case study such as impedance matching, gradient-based optimization procedures, and the minimax formulation for circuit optimization.

Following the definition of the project, specifications to work on the 868MHz Industrial, Scientific, and Medical radio band (ISM band) and the applied guidelines of the long-range SoC for impedance matching of the Power Amplifier (PA transmitter) and Low Noise Amplifier (LNA receiver) paths based on the optimal impedance data. This section presents a series of simulation results based on the reflection coefficient to demonstrate the effects on the impedance-matching network due to the addition of filters and transmission lines.

These results include further specifications in the design to mitigate the effects of unwanted frequencies based on reflection coefficient responses. To continue with the formulation of an objective function that will serve to apply the classical optimization followed by the presentation of optimization results.

It is intended to implement classical optimization to overcome the disturbances of the impedance matching caused by the addition of mandatory filters to the PA and the balun circuit of LNA paths, nonetheless, it is unavoidable to tune the lumped component values in the actual PCB, by employing laboratory equipment such as a spectrum analyzer to confirm output power. This time-consuming task could be eased by creating fine models using advanced circuit simulators that typically include a good enough set of algorithms for optimization. However, it was decided for this project to implement basic algorithms of classical optimization methods since the stand-alone

optimization algorithms make it possible to customize cost functions from different simulators' analysis responses

.

Contents

1. Introduction

LoRa is a long-range modulation radio working on the sub-gigahertz ISM band, for instance, EU863-EU870 MHz in Europe and US902-US928 MHz in North America. Over the past decade, the demand for LoRa radios has increased not only for industrial and commercial applications but also is appealing to the maker community for long-range application IoT projects. Although LoRa transceivers can be found as small form factor modules with a completely characterized signal chain and antenna port that can be simply soldered on PCBs using castellated pins, these modules may exceed the application requirements when modest applications are desired. Additionally, it may be of interest to have a smaller form-factor PCB or to reduce costs by having a different PCB stack-up. The latter is a good example of impedance matching and optimization design, being one of the motivations to develop this case study.

The guidelines from the AN5457 application note [1] are implemented, detailing the typical RF matching and filtering circuit for STM32WL Series devices and how to become compliant with certification standards by applying filtering circuits. Additionally, information on the load-pull analysis of the PA and LNA pins of the STM32WL SoC is applied for initial calculations. The load-pull analysis is useful to determine the maximum possible output power given a load impedance. Even though 50Ω is a common reference impedance, it is uncommon to get this value of impedance from the PA and LNA pins due to design or technology constraints, thus the optimal impedance value is required to design the matching network.

The impedance matching technique presented throughout this essay is narrow band, it relies on conjugate matching, given that both source and load impedances are complex [2]. This can be referred to in Chapter 1, where also concepts such as one-port network and reflection coefficient are covered.

An overview of optimization concepts is presented in Chapter 2, one can find the line search gradient-based algorithms, and how the exact line search was implemented for this study. In the same chapter, the formulation for unconstrained optimization is also presented, as a method to limit the optimization space by using box constraints. The latter is of big importance to this project as one can see in the Optimization Results chapter.

The circuits of the transmit and receive paths presented in Chapter 4 are modeled as a one-port network; this simplifies the analysis by using plain equations or graphical methods such as Smith Charts to obtain initial values of the lumped components. By using the available stack-up information for 50Ω control impedance from a low-cost PCB manufacturer, a transmission line model is included in the matching network circuits.

Based on the results of the final circuit models, the design specifications are updated to minimize the disturbances on the reflection coefficient by the interaction of the different filtering stages. While it is not the purpose of this project to modify the proposed topology presented in [1], the specifications are updated based on the circuit capabilities. That said, it is the objective to reduce the disturbances on the reflection coefficient as much as possible for the given circuit topologies. This can be further reviewed in Chapter 5.

A cost function is defined in Chapter 6, it is based on a minimax formulation from the S-parameter and transient initial responses of the PA and LNA. The essay continues presenting optimization results after applying gradient-based and Nelder-Mead methods testing different initial values or seeds. The Optimization Results section details the presented obstacles regarding convergence and how this was mitigated.

To finalize this work, at the end of the essay a brief conclusion and future work suggestions are presented.

2. Defining the Problem

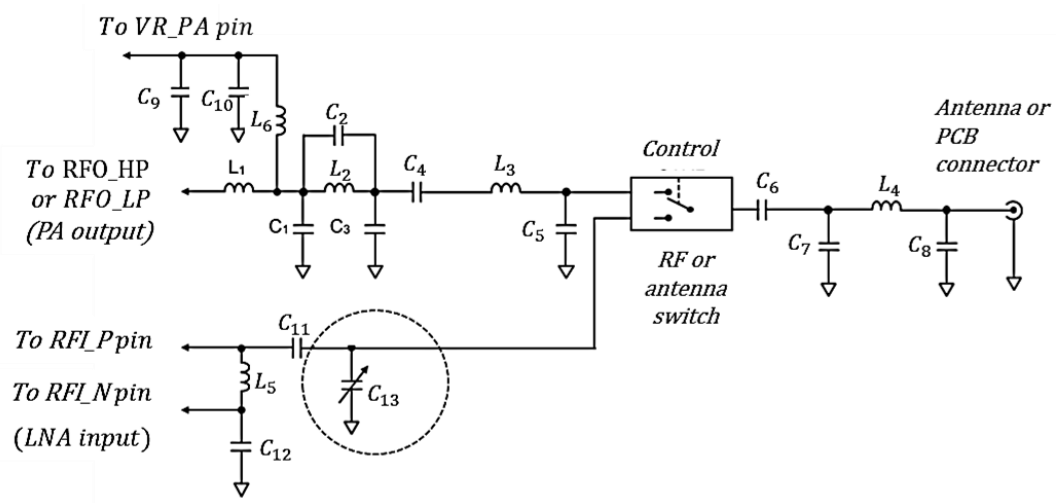

Fig. 2-1 Transmit and receive chain topologies. The transmit and receive paths are isolated as the transceiver works in half-duplex mode. The image is taken from [1].

LoRa transceivers work in half-duplex mode by isolating the transmit and receive paths. This means that each path can be connected to a transmit and receive antenna or can be isolated by including an SPDT RF switch between the transmitter output and the receiver input. The reference design presented by STMicroelectronics and other vendors of LoRa radio transceivers is displayed in Fig. 2-1. Bearing in mind, it is not the intention of this project to modify the suggested network impedance and filtering topology, but rather to assist to find the optimum values to overcome the harmonic filtering addition affecting the reflection coefficient.

To simplify the analysis, the RF switch block is represented by a generic 50 Ω port. The system is intended to work at the EU868MHz frequency bands and the STM32WL UFQNFPN48 package. From the load-pull analysis:

- Transmitter: +14dBm using RFO_LP pin. Optimal impedance value 15.27 + j1.27Ω.
- Receiver: RSSI -70dBm. Optimal impedance value 52+j102 Ω.

3. RF MATCHING CONCEPTS

TABLE I
JLC2313 STACK-UP. 4 LAYER PCB 50Ω CONTROLLED IMPEDANCE

Layer	Material Type	Thickness	Notes
Top Layer1	Copper	1.38 mil	
Prepreg	2313*1	3.94 mil	
Inner Layer2	Copper	0.69 mil	51.18 mil (with copper core)
Core	Core	49.8 mil	
Inner Layer3	Copper	0.69 mil	
Prepreg	2313*1	3.94 mil	
Bottom Layer4	Copper	1.38 mil	

Given the optimal impedance values and the frequency of interest, the design of the matching network can be implemented. All formulae and equations for the lumped values calculations are based entirely on [1].

The stack-up applied for this case study is presented in TABLE I. The transmission line models used for the resulting circuits are derived from *Top Layer1* and Inner *Layer 2* as a reference, the manufacturer indicates a 5.78mil trace width to achieve 50Ω impedance control with this stack-up. I

In addition, data from the supplier regarding the 2313 prepreg thickness is the usage of 4.5mil for external layers in its place of the depicted nominal value of 3.94 mils [11].

- Electrical permittivity ε_r=4.05
- Substrate loss tangent $\tan\delta$=0.015
- Copper electrical conductivity $\sigma = 58.7x10^6 \frac{S}{m}$
- Thickness t=1.4mil
- Height H=3.5mil
- Microstrip width W_s=5.78mil

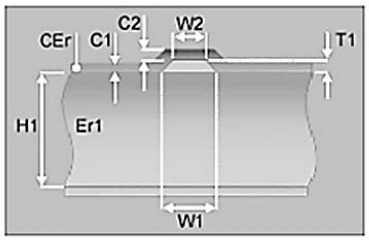

H1: 3.5 **Er1: 4.05**
T1: 1.40 **C1: 0.80**
C2: 0.50 **CEr: 3.80**

Fig. 2-2 Cross-section of the microstrip model according to stack-up vendor. Recommended trace width for JLC2313 prepreg to comply with 50 **Ω** impedance control is 5.78 mil.

With a maximum reflection coefficient denoted by the $|S_{11}|$ and response at f_0=868MHz. the specifications are defined as $|S_{11}| < 0.1$ for $f_L < f_0 < f_H$ where f_L=860MHz and f_H=880MHz for both PA and LNA paths.

3. RF Matching Concepts

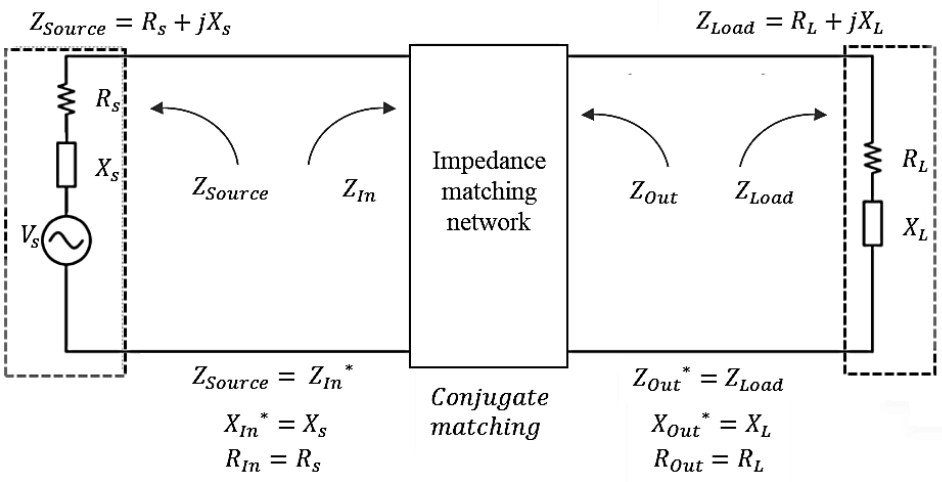

Fig. 3-1 Conjugated impedances representing a matching network between a source impedance (transmitter) and load impedance (antenna). The image is taken from [1].

Narrowband impedance matching relies on conjugate matching, given that both source and load impedances are complex. Fig. 3-1 depicts a source with impedance $Z_{Source} = R_S + jX_S$ driving a load impedance $Z_{Load} = R_L + jX_L$, the maximum power transfer to Z_{Load} and minimum reflection from it is achieved when $R_S = R_L$ and $X_L = -X_S$ in other words, for a complex source impedance, the maximum power transfer is obtained when $Z_{Source} = Z_{Load}^*$.

A mismatch impedance on the path of a transmission line when a signal flows from the source to the load will cause part of the signal to be reflected from the load to the source. To express the reflected waves, return loss, VSWR, and reflection coefficient are commonly used parameters indicating the performance of the impedance matching network. The reflection coefficient Γ can be represented by the relationship between the load impedance and the characteristic impedance of the transmission line.

$$\Gamma = \frac{Z_{Load} - Z_o}{Z_{Load} + Z_o} \tag{3-1}$$

3. RF MATCHING CONCEPTS

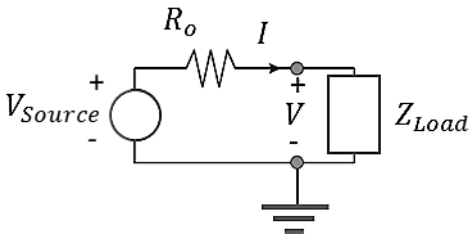

Fig. 3-2 Voltage source driving a one-port load impedance. The voltage source equivalent Thévenin resistance is R_o, also known as the reference impedance Z_o of the one-port network.

The reflection coefficient of an impedance is unique for a given impedance function, and conversely, a unique impedance derives from a specific reflection coefficient [3]. The reflection coefficient can also represent the Cartesian impedance plane by magnitude and phase. The magnitude of Γ can be represented as

$$\rho=\frac{Z_{Load}-R_o}{Z_{Load}+R_o}=\frac{Z_{ln}-1}{Z_{ln}+1} \tag{3-2}$$

where

$$Z_{ln}=\frac{Z_{Load}}{R_o} \tag{3-3}$$

representing the load impedance normalized to the system reference impedance.

Antenna-matching network performance can be evaluated by the reflection coefficient ρ. To demonstrate this, consider the one-port network of Fig. 3-2. In scattering theory, the Thévenin impedance is represented by R_o is often called reference impedance Z_o of the one-port network. The current I conducted by the load Z_{Load}, can be represented as the sum of the incident current I_i and the reflected or scattered current I_r

$$I=I_i - I_r \tag{3-4}$$

In the last equation, I_i is defined as the value of the current I for a load impedance Z_{Load} that is matched to the one-port reference impedance, R_o, so $Z_{Load}\equiv R_o$. Then, the incident current can be obtained as

$$I_i=\frac{V_{Source}}{2R_o} \tag{3-5}$$

hence the reflected current I_r follows as

$$I_r = I_i - I = \frac{V_{Source}}{2R_o} - \frac{V_{Source}}{R_o + Z_{Load}} = \left(\frac{Z_{Load} - Ro}{Z_{Load} + Ro}\right)\frac{V_{Source}}{2R_o} \tag{3-6}$$

Notice that the left side of the final equation is the reflection coefficient Γ from (3-1) as R_o is the reference $Z_o$impedance.

Given (3-2) and (3-5) the relationship between the current and the reflection coefficient on (3-6) can be presented as

$$I_r = \rho I_i \tag{3-7}$$

so

$$I = (1 - \rho)I_i \tag{3-8}$$

Verifying that the only current supplied by the signal source is the incident current if no reflections exist employing ρ=0. This resembles terminating the load impedance matched to the reference impedance.

The same analysis can be done for the load voltage V decomposed as the incident V_i and reflected V_r components with

$$V = V_i + V_r \tag{3-9}$$

For an incident wave, the voltage V for a matched load impedance to the circuit reference impedance is

$$V_i = \left(\frac{Z_{Load}}{R_o + Z_{Load}}\right) V_s \Big|_{Z_{Load}=R_o} = \frac{V_{Source}}{2} \tag{3-10}$$

The scattered load voltage component is

$$V_r = \left(\frac{Z_{Load} - R_o}{Z_{Load} + R_o}\right)\frac{V_{Source}}{2} = \rho V_i \tag{3-11}$$

Analogous to (3-8) the incident voltage is the net load voltage when no reflections occur.

$$V = (1 + \rho)V_i \tag{3-12}$$

From the above, it is reliable to evaluate the performance of the impedance-matching circuit based on the reflection coefficient of the one-port network.

4. Optimization Concepts

Classical or conventional optimization methods including line search and trust region strategies pursue to minimize (4-1)

$$\mathbf{x}^* = \arg\min_{\mathbf{x}} u(\mathbf{x}) \tag{4-1}$$

where $x \in R^n$ and $u: R^n \rightarrow R$.

The objective function defined as $u(\mathbf{x})$ represents the target function that includes the optimization variables $\mathbf{x}$.

From [4] to restrict the optimization space, an unconstrained optimization problem can be transformed by using box constraints. To set upper and lower boundaries for the optimization variables, this project implements:

$$x_i^{lb} \leq x_i \leq x_i^{ub} \tag{4-2}$$

With a transformation variable to $\mathbf{z}$, it is now the intention to solve

$$\boldsymbol{z}^* = \arg\min_{\mathbf{z}} u(\mathbf{z}) \tag{4-3}$$

For (4-2) the transformation variable is:

$$x_i = \frac{1}{2}\left(x_i^{lb} + x_i^{ub}\right) + \frac{1}{2}\left(x_i^{lb} - x_i^{ub}\right)\sin z_i \tag{4-4}$$

Optimization methods that use derivative information are more effective when the function is continuous in the first and second derivatives (Gradient methods). On the other hand, methods that use only function evaluations are more suitable for problems that are very nonlinear or have many discontinuities (search methods) [5].

The gradient methods are descent methods where the linear approximation is implemented given $u(\mathbf{x_i}+\mathbf{d})$ as a function of the vector $\mathbf{d}$, the search is done with a direction $-\nabla u(\mathbf{x_i})$. In other words, the minimum is searched with a vector having a direction of the negative of the gradient.

Both Conjugate Gradients and Quasi-Newton algorithms implemented in this project are methods that only need the first derivative of the function, thus are commonly used in a great variety of fields, like circuit optimization. On the other hand, the Nelder-Mead, or downhill

simplex method, is a line search numerical method for twice differentiable and unimodal problems [5]. The Nelder-Mead algorithm is also applied in this study to compare against the conjugate-based algorithms.

4.1. Conjugate Gradient Algorithm

The Conjugate Gradient Method is based on the linear combination of the steepest descent direction and the previous direction. This study implements the algorithm from [6]

begin

$i=0$, $x_i=x_0$, $\beta_i=0$

repeat until *StoppingCriteria*

$\mathbf{d}_i=-\nabla u(\mathbf{x}_i)+\beta_i\mathbf{d}_{i-1}$

$\alpha_i=\text{LineSearch}(u,\mathbf{x}_i,\mathbf{d}_i)$

$\mathbf{x}_{i+1}=\mathbf{x}_i+\alpha_i\mathbf{d}_i$

$i=i+1$

$\beta_i=\text{UpdateBeta}(u, \mathbf{x}_i , \mathbf{x}_{i-1})$

end

From the above, the value of β_i is selected such that $\mathbf{d}_i$ and $\mathbf{d}_{i-1}$ are conjugate directions. To update the value β_i the Fletcher-Reeves (F-R) and Polak-Ribiére (P-R) formulas can be applied. The latter is implemented in this project.

F-R formula

$$\beta_{i+1} = \frac{\nabla u(\mathbf{x}_i)^T \nabla u(\mathbf{x}_i)}{\nabla u(\mathbf{x}_{i-1})^T \nabla u(\mathbf{x}_{i-1})} \tag{4-5}$$

P-R formula

$$\beta_{i+1} = \frac{[\nabla u(\mathbf{x}_i)-\nabla u(\mathbf{x}_{i-1})]^T \nabla u(\mathbf{x}_i)}{\nabla u(\mathbf{x}_{i-1})^T \nabla u(\mathbf{x}_{i-1})} \tag{4-6}$$

4.2. Quasi-Newton Algorithm

Newton's method finds a minimizer of a quadratic in n-dimensional space in one iteration. However, it requires solving the Hessian of the function $\mathbf{H}(u(\mathbf{x_i}))\ \mathbf{d}_i = -\nabla u(\mathbf{x_i})$ for $\mathbf{d}_i$ demanding extra computational costs. For that reason, the Quasi-Newton method is commonly used as it is easier to approximate the Hessian (or its inverse) using a matrix. It is a powerful method for solving unconstrained optimization problems. The implemented generic Quasi-Newton algorithm from [6] in this project is

begin

$i=0,\ x_i=x_0,\ \beta_i=0$

repeat until *StoppingCriteria*

$\mathbf{d}_i=-\nabla u(\mathbf{x_i})+\beta_i\mathbf{d}_{i-1}$

$\alpha_i=\text{LineSearch}(u,\mathbf{x}_i,\mathbf{d}_i)$

$\mathbf{x}_{i+1}=\mathbf{x}_i+\alpha_i\mathbf{d}_i$

$i=i+1$

$\beta_i=\text{UpdateBeta}(u,\ \mathbf{x}_i\ ,\ \mathbf{x}_{i-1})$

end

To update the value β_i the Broyden, Fletcher, Goldfarb, and Shanno (BFGS) and Symmetric-Rank one (SR1) are implemented.

SR1 formula

$$\mathbf{B}_{i+1} = \mathbf{B}_i \frac{(\mathbf{y}_i-\mathbf{B}_i\mathbf{s}_i)(\mathbf{y}_i-\mathbf{B}_i\mathbf{s}_i)^T}{(\mathbf{y}_i-\mathbf{B}_i\mathbf{s}_i)^T\mathbf{s}_i} \tag{4-7}$$

BFGS formula

$$\mathbf{B}_{i+1} = \mathbf{B}_i - \frac{\mathbf{B}_i\mathbf{s}_i\mathbf{s}_i^T\mathbf{B}_i}{\mathbf{s}_i^T\mathbf{B}_i\mathbf{s}_i} + \frac{\mathbf{y}_i\mathbf{y}_i^T}{\mathbf{y}_i^T\mathbf{s}_i} \tag{4-8}$$

where $\mathbf{s}_i = \mathbf{x}_{i+1} - \mathbf{x}_i$, $\mathbf{y_i}=\nabla u(\mathbf{x_{i+1}})- \nabla u(\mathbf{x_i})$.

4.3. Line Search

The applied Line Search algorithm is based on Matlab's *fminbnd* command to minimize scalar unidimensional functions. It employs Golden Section and the quadratic interpolation methods. When solving (4-1) to find the descent search direction $\mathbf{d}_i$ used for the next $\mathbf{x}_{i+1}$:

$$\alpha^* = \arg\min_{\alpha>0} u(\mathbf{x}_i+\alpha\mathbf{d}_i)\alpha^* = \arg\min_{\alpha>0} u(\alpha) \tag{4-9}$$

then

$$\mathbf{x}_{i+1} = \mathbf{x}_i + \alpha^* \mathbf{d}_i \tag{4-10}$$

The implemented line search algorithm has a unitary direction.

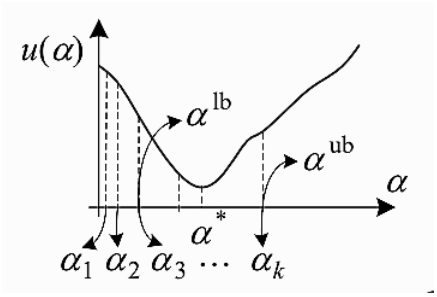

Fig. 4-1 Screening representation to set lower and upper boundaries represented by $\alpha^{lb}$and α^{ub} when minimizing u(α). The image is taken from [6].

$$\mathbf{x}_{i+1} = \mathbf{x}_i + \alpha^* \frac{\mathbf{d}_i}{\|\mathbf{d}_i\|} \tag{4-11}$$

It is possible to bound the exact line search. The screening to define bounds algorithm from [7] [8]is implemented for this project:

$$\{\alpha^{lb}, \alpha^{ub}, k\} = \text{LineSearchBounds}(u, \mathbf{x}_i, \mathbf{d}_i) \tag{4-12}$$

for

$$u: \Re \to \Re; \mathbf{x}_i, \mathbf{d}_i \in \Re^n;\ \alpha^{lb}, \alpha^{ub}, k \in \Re$$

begin

initialize r, α_{min}

$k = 1;\ \alpha = 0;\ u = u(\alpha);$

$\alpha = \alpha_{min};\ u_{new} = u(\alpha);\ k = k + 1;$

while $u > u_{new}$

$u = \mathrm{u}_{\mathrm{new}}$

$\alpha = r\alpha$

$\mathrm{u}_{\mathrm{new}} = u(\alpha)$

k= k + 1

end

if k = 2 **then** $\alpha^{\mathrm{lb}} = 0$

else $\alpha^{\mathrm{lb}} = \frac{\alpha}{r^2}$

end

Therefore, the screening is done at $\alpha = r^{\mathrm{k}}(\alpha_{\mathrm{min}})$. The objective function definition for this project is covered in Chapter 6.

4.4. MiniMax Formulation for Circuit Optimization

From the definition of a general formulation of an optimization design given by [9], a problem of circuit design with the desired response $\mathbf{R}^* \in \mathrm{R}^n$ in terms of design specifications or goals, can be formulated as

$$\mathbf{x}^* = \arg\min_{\mathbf{x} \in X} \mathrm{U}(\mathbf{R}(\mathbf{x})) \tag{4-13}$$

where

$\mathbf{x}^*$ is the optimal design

X is the feasible region,

U is a suitable objective function

$\boldsymbol{R}(\mathbf{x}^*) = \mathbf{R}^*$ can be different circuit models. The independent variables such as frequency, time, bias voltages, and others are contained in the vector ψ.

The minimax formulation to circuit design optimization [10] where an error function $e_k(\mathbf{x})$ is defined for every upper and lower specification, every response, and independent variable sample (frequency, time, etc). Each equality specification can be given by upper and lower boundary specifications.

A general minimax formulation is presented as

$$\mathbf{x}^* = \arg\min_{\mathbf{x} \in X} \mathrm{U}(\mathbf{R}(\mathbf{x})) \_ \mathbf{x}^* = \arg\min_{\mathbf{x}} \max \{ \ldots e_k(\mathbf{x}) \ldots \} \tag{4-14}$$

where a negative value in the $e_k(\mathbf{x})$ error function, implies that the corresponding design specification is satisfied. If a positive number still exists in $e_k(\mathbf{x})$, the design specification is not achieved.

$$e_k(\mathbf{x}) = \begin{cases} \dfrac{R_k(\mathbf{x})}{S^{ub}+\varepsilon} - 1 \text{ for all } k \in I^{ub} \\ 1 - \dfrac{R_k(\mathbf{x})}{S^{lb}+\varepsilon} \text{ for all } k \in I^{lb} \\ \dfrac{| R_k(\mathbf{x}) - S^{eq}|}{s^{ub}+\varepsilon} - 1 \text{ for all } k \in I^{eq} \end{cases} \tag{4-15}$$

Where $R_k(\mathbf{x})$ is the k-th model response at point $\mathbf{x}$, $S^{ub}{}_k > 0$ and $S^{lb}{}_k > 0$ are the upper and lower bound specifications, $S^{eq}{}_k$ are equality specifications. The index sets are I^{ub}, I^{lb} and I^{eq} and ε is an arbitrarily small positive number. The minimax formulation attempts to make all errors as negative as possible.

A basic stopping criterion monitors the error function $U(\mathbf{x}^*)$, to finalize the optimization process when any of the following conditions are met.

The relative change of the optimization variables

$$\|\mathbf{x}_{i+1} - \mathbf{x}_i\|_2 < \varepsilon_x(\|\mathbf{x}_i\|_2 + \varepsilon_x) . \tag{4-16}$$

The second condition is the function tolerance

$$\|\nabla u(\mathbf{x}_i)\|_2 < \varepsilon_g . \tag{4-17}$$

The third condition is the maximum iterations

$$i > i_{max} . \tag{4-18}$$

Combining (4-16) and (4-17) with $U(\mathbf{x}^*) < 0$

$$\begin{gathered} \|\mathbf{x}_{i+1} - \mathbf{x}_i\|_2 < \varepsilon_x(\|\mathbf{x}_i\|_2 + \varepsilon_x) \wedge U(\mathbf{x}^*) < 0 \\ \vee \|\nabla u(\mathbf{x}_i)\|_2 < \varepsilon_g \wedge U(\mathbf{x}^*) < 0 \\ i > i_{max} \end{gathered} \tag{4-19}$$

5. Matching and Filtering Networks

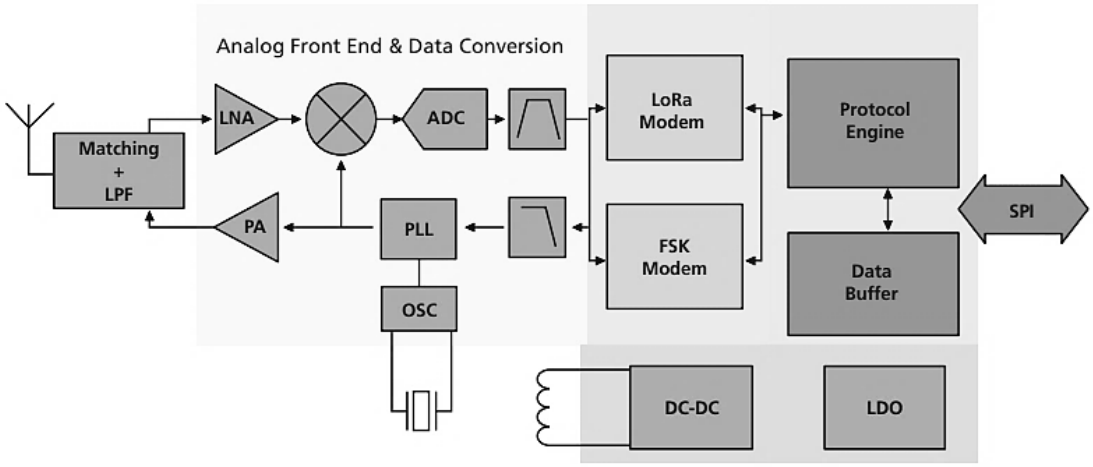

Fig. 5-1 Generic LoRa transceiver block diagram. The analog front end, matching, and filtering blocks are common with the STM32WL and other SoCs supporting LoRa modulation.

As part of the analog front end and data conversion section of the generic block diagram of a LoRa radio presented in Fig. 5-1, it is visible the LNA (input) and the PA (output) composed of the receive and transmit pins. Similar to any RF front end, a matching and filtering section outside the radio must be incorporated. In this chapter, the transmit and receive paths are described, including the functionality and design of each block of the matching and filtering elements.

5.1. Transmitter Network Analysis

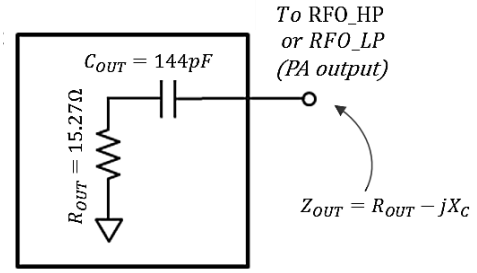

Fig. 5-2 Equivalent circuit of the PA output pin impedance for the package UFQFPN48, output power of14dBm at 868MHz. The series capacitor indicates a negative reactance.

The STM32WL includes two output pins noted as RFO_HP and RFO_LP for high output power and low output power respectively. The latter is used for the following analysis; since the low output power can be programmable up to +15dBm, the information from the load-pull analysis corresponding to +14dBm is sufficient

5.1.1 Transmitter Impedance Matching

As for the transmit network application presented in Fig. 2-1 the filtering used for the VR_PA composed by $C_{9,}$ C_{10} and L_6 is excluded from circuit analysis. On the other hand, the DC-blocking capacitor C_4 is fixed to 68pF.

To model the transmit path as a one-port network it is required to use the conjugate value of the optimal impedance from the load-pull analysis.

$$Z_{out} = Z_{optimal}^{*} = 15.27\text{-}j1.27\Omega \qquad (5\text{-}1)$$

A negative value in the reactance X_C indicates a capacitive behavior. C_{out} can be calculated as

$$C_{out} = \frac{1}{2\pi f_0 X_C} = \frac{1}{2\pi * 868MHz * 1.27} = 144.37pF \qquad (5\text{-}2)$$

The basic approach is to calculate the L-C matching network consisting of L_1 and C_1 as seen in Fig. 2-1.

$$L_1=\frac{50m}{m^2+1}+X_C \tag{5-3}$$

where

$$m=\sqrt{\frac{50}{R_{out}}-1}=\sqrt{\frac{50}{15.27}-1}=1.508 \tag{5-4}$$

then

$$L_1=\frac{50*1.508}{(1.508)^2+1}+1.27=4.45nH \tag{5-5}$$

To calculate C_1

$$C_1=\left|\frac{1}{2\pi f_0}\frac{\sqrt{\frac{R_{out}}{50}(1+m^2)-1+m}}{R_{out}(1+m^2)}\right| \tag{5-6}$$

$$C_1=\left|\frac{1}{2\pi f_0}\frac{\sqrt{\frac{15.27}{50}(1+1.508^2)-1+1.508}}{15.27(1+1.508^2)}\right|=5.53pF$$

It can be seen in Fig. 5-3 that L_1 approaches to the middle 50Ω circle of the Smith chart, as for C_1 reaching the center, indicating the correct impedance matching. More information about the reflection coefficient can be seen in the Smith chart based on the frequency sweep seen by the generator G of the circuit in Fig. 5-4. Keeping in mind that at the desired frequency of 868MHz the impedance must be the closest possible to the center of the Smith chart, indicative of the 50Ω characteristic impedance for a correctly matched impedance.

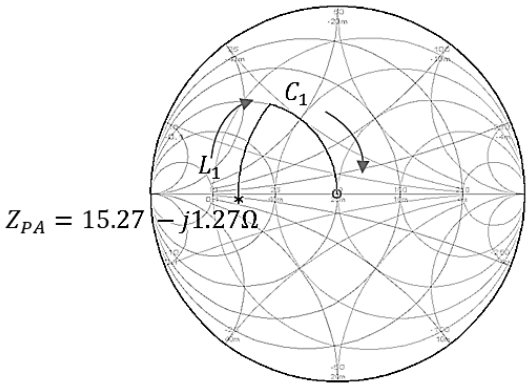

Fig. 5-3 L_1 and C_1effects seen in the Smith chart to match the impedance of the PA output. Z_{PA}corresponding to the PA impedance output being the conjugate complex of $Z_{optimal}$.

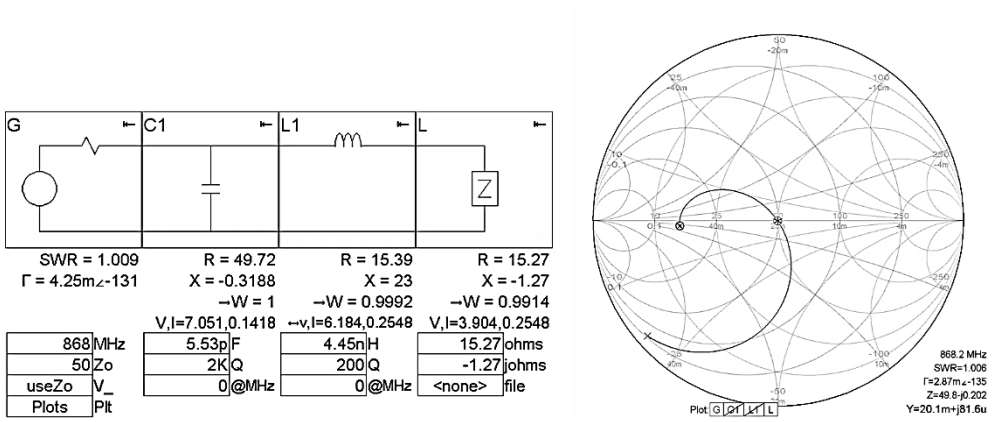

Fig. 5-4 To the left, the circuit representing the impedance matching composed by $L_1$and C_1 with a load of Z_{PA} =15.27-j1.27Ω. The frequency sweep to the right shows an impedance of 49.8 – j0.202 Ω at approximately 868MHz.

5.1.2 Transmitter Filters

Because the RF PA is a non-linear system, there are spurious signals that distort the input of the RF signal, as well as the harmonic contents of the output signal. The harmonic contents must be limited to be compliant with the regulations of the usage of the electromagnetic spectrum. It is illustrated in Fig. 5-5 some of the disturbances affecting the fundamental frequency that could become a violation of these regulations. The filtering stage must limit the additional frequency components with a safe margin below the noise limit established by the regulatory agencies.

A notch filter is included on the transmit path, composed by L_2 and C_2 as seen in Fig. 2-1. To implement this filter, the second harmonic H_2 is considered as the cut-off frequency H_2=2 x 868MHz=1.7326GHz.

From [1] a recommended value for L_2 is selected as $\frac{3}{4}L_2$=3.34nH.

The resonant frequency can be determined as

$$2\pi H_2=\frac{1}{\sqrt{L_2C_2}} \tag{5-7}$$

From which,

$$C_2=\frac{1}{(2\pi H_2)^2 L_2} \tag{5-8}$$

$$C_2=\frac{1}{(1.736)^2(3.34)}=2.52\text{pF}$$

The simulation of the notch filter depicted in Fig. 5-6 has a good response to attenuate H_2, at the same time, the effects of the reflection coefficient are notorious. Adding the notch filter to the matching network shifts the impedance towards the inductive area of the Smith chart as seen in Fig. 5-7.

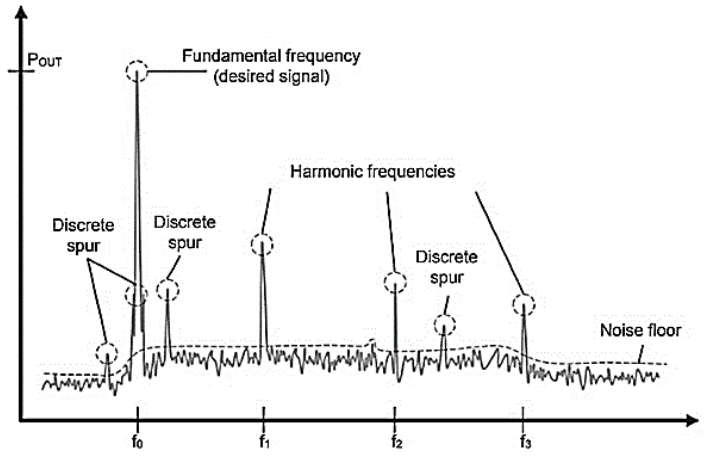

Fig. 5-5 Representation of fundamental signal, harmonics, and spurious power over frequency. The image is taken from [1].

5. MATCHING AND FILTERING NETWORKS

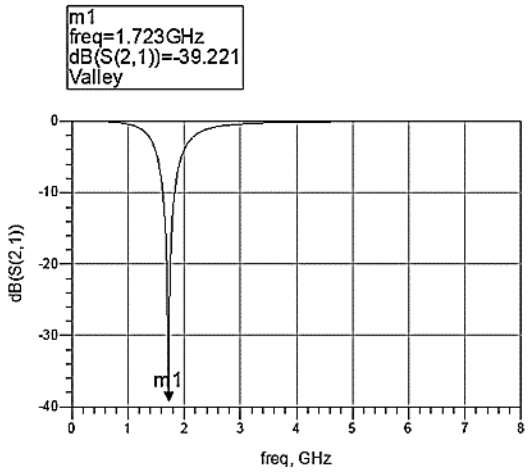

Fig. 5-6 Notch filter $|S_{21}|$ response composed by L_2 and C_2 to remove H_2=1.7326GHz, the attenuation is around -22dB.

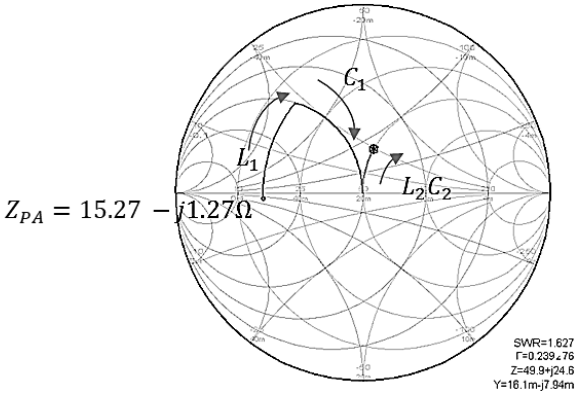

Fig. 5-7 Disturbance on the transmit impedance matching network due to the inclusion of the notch filter composed by the parallel connection of L_2 and C_2.

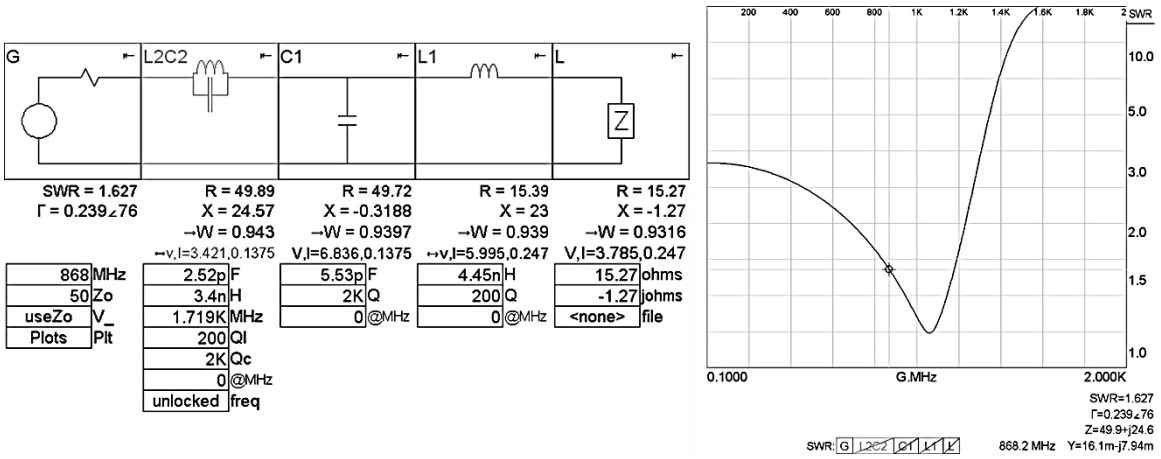

Fig. 5-8 To the left, the circuit representing the impedance matching composed by $L_1$and C_1 and the inclusion of the notch filter with a load of Z_{PA} =15.27-j1.27Ω. The $|S_{11}|$ response to the right showing the shifting of the reflection coefficient to about 1GHz.

The reflection coefficient magnitude ρ is higher, around 0.23 for the expected frequency of 868MHz, moreover, there may be a coupling below 500MHz due to the decreasing tendency of the $|S_{11}|$. This can be observed in Fig. 5-8.

From a practical approach, the fine-tuning process could start with the addition of the notch filter. It could be done by measuring the output power to verify the rejection of H_2, and slightly increasing the values of C_1 [1] minding the impact on the output power. Then again, this project relays on optimization algorithms to modify the value of C_1 based not only on the notch filter and the L_1C_1impedance circuit, but the concurrence of the rest of the elements of the transmit chain.

Adding C_3 as per Fig. 5-9 may reduce the impact of the notch filter. According to AN5457, STMicroelectronics recommends values of C_3 0.5 to 1.5 pF.

At this moment, no tunning is performed, it is preferred to continue with the implementation of the low pass filter consisting of C_3, L_3 and C_5 from Fig. 2-1.

Notice the topology illustrated in Fig. 5-10 corresponding to a π ladder filter, this is useful as it requires just one inductor rather than other filter topologies like T-ladder, thus reducing the parasitic effects.

To determine the values of the low-pass filter

$$L_3=\frac{50}{2\pi f_0} \tag{5-9}$$

$$L_3 = \frac{50}{2\pi 868 \text{x} 10^6} = 9.2\text{nH}$$

And the combination of capacitors values

$$C' = C'' = \frac{0.95}{(50)2\pi f_0} \tag{5-10}$$

$$C' = C'' = \frac{0.95}{(50)2\pi 868 \text{x} 10^6} = 3.5\text{pF}$$

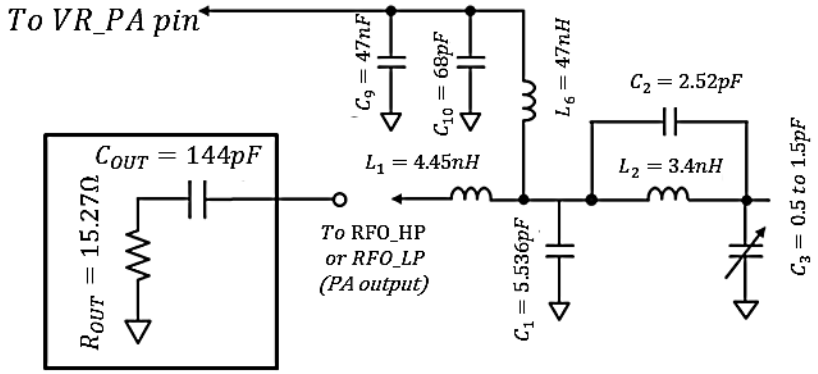

Fig. 5-9 The addition of C_3 may reduce the impact of the notch filter. Recommended values from [1] with a range of 0.5pF to 1.5pF.

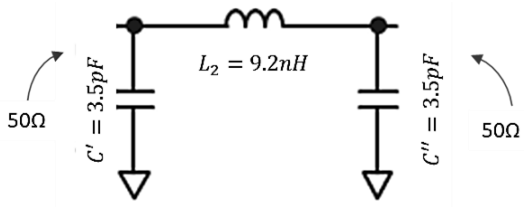

Fig. 5-10 Low-pass π filter with 50Ω input and output impedances. The image is taken from [1].

The low-pass filter response is of the Chebyshev type: a zero can be set at H_1 with a good roll-off in the stopband [1]. At 868MHz the forward transmission $|S_{21}|$ is around -70e^{-6} dB as a good cut-off frequency, up to 8GHz the attenuation is ideally sufficient.

The purpose of C_4 is to bock DC signals between C_3 and C', its effect on impedance matching is neglected for this analysis. Let $C_3 = 0.8$pF, to reduce the real state on the PCB the values of C_3 and C' are combined as part of the π ladder filter. The new value is C_3=C_3 +

$C^{'}$ = 0.8+3.5 = 4.3pF. The final transmission network impedance matching circuit is shown in Fig. 5-12.

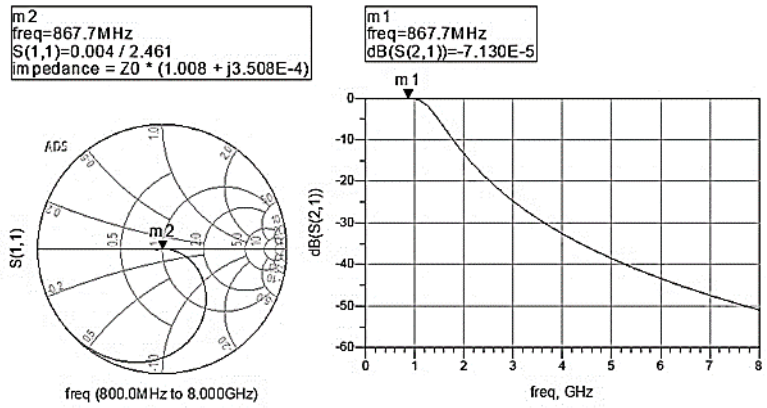

Fig. 5-11 Low-pass π filter response. The filter is designed for a cut-off frequency H_1=868MHz. $|S_{21}|$ is around -70e^{-6}dB. Notice the 868MHz is on the center of the Smith chart.

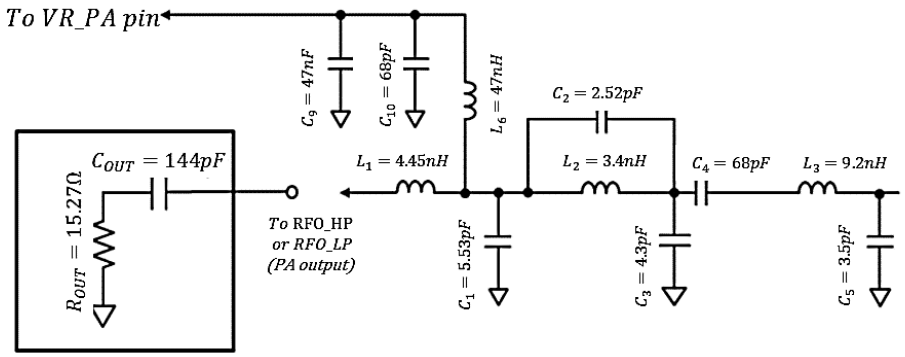

Fig. 5-12 Complete circuit of the matching network and filtering of the PA. The value of C_5 should be decided based on the required RF switch. Because of the parasitic input capacitance of the switch, its value may have to decrease to get the correct output power [1].

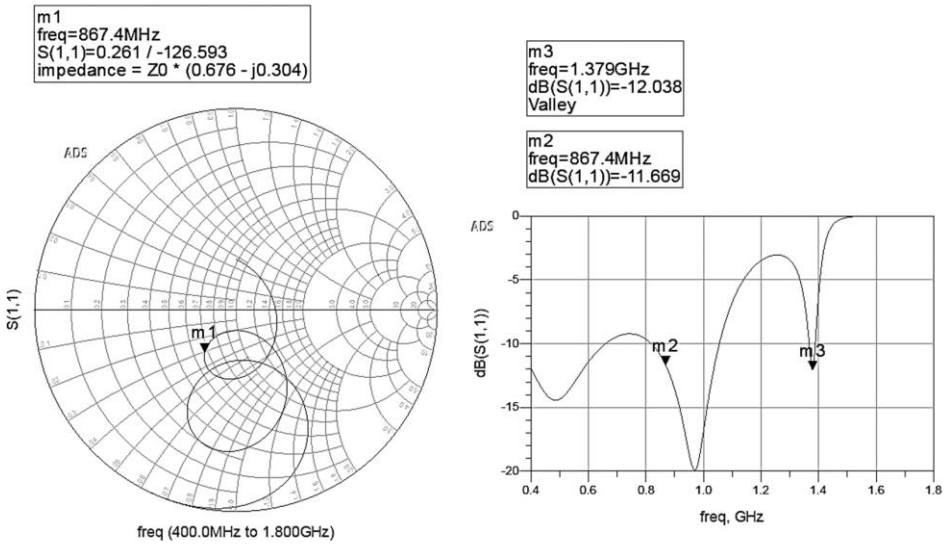

Fig. 5-13 Disturbances on the frequency sweep of the impedance matching network due to the addition of the filtering stage. From the response of $|S_{11}|$ there is a coupling near 1.4GHz.

Some RF switches have parasitic input capacitance that must be considered for the value of C_5. To verify the final value of C_5, one can measure the output power without the switch and adjust the value of C_5 to get the right output power. On the other hand, to simplify the analysis, this study is done with an ideal 50Ω impedance port due to its practicality when mapping to any commercial microwave analyzer.

Even if the component models are ideal and the effects of the PCB are also overlooked for this simulation, it is noticeable the disturbance of the matching network illustrated in Fig. 5-13. Not only the central frequency is shifted to the right, but there is a coupling around 1.4GHz.

The calculated values of the lumped components used in the optimization phase of this project can be seen in TABLE II. The impact of PCB transmission lines is considered in a later analysis presented in the upcoming chapters. For the time being, the design of the receive path is explained next.

TABLE II TRANSMITTER IMPEDANCE MATCHING AND FILTERING CIRCUIT VALUES OF LUMPED COMPONENTS. FIRST SEED FOR OPTIMIZATION.

PA transmitter calculated values
L_1=4.45nH
C_1=5.53pF
C_2=2.52pF
L_2=3.4nH
C_3=4.3pF
L_3=9.2nH
C_5=3.5pF

5.1. Receiver Network Analysis

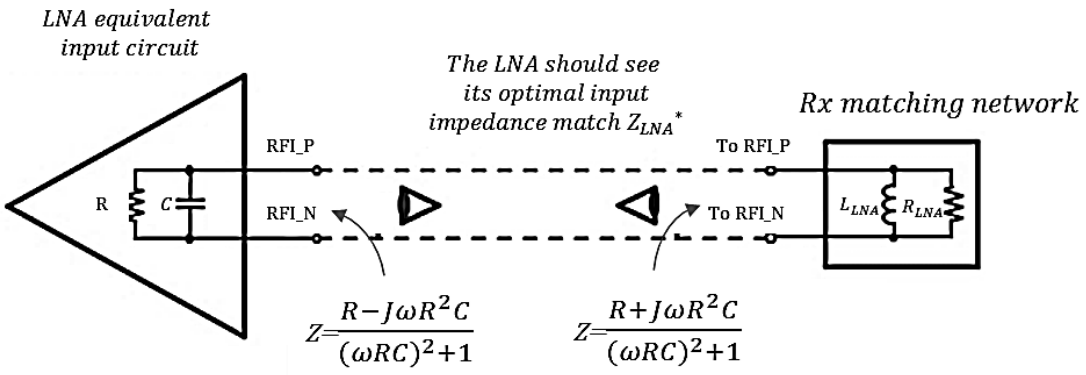

Fig. 5-14 LNA equivalent circuit and impedance with the required matching network (complex conjugate). The image is taken from [1].

The receiver section of the STM32WL consists of an LNA, it has an equivalent input impedance with a negative reactance, therefore, the equivalent circuit is the parallel connection of a resistor with a capacitor from Fig. 5-14. Recalling that the impedance matching of the LNA optimal impedance is the complex conjugate of its impedance. As illustrated in the previous figure, the LNA input circuit should see its optimal input impedance match Z_{LNA}^* (optimal). From the load-pull analysis, the LNA optimal impedance of the required package, frequency, and output power is 52+j102Ω, its complex conjugate should be 52 - j102Ω.

To confirm the negative reactance of the optimal $Z_{LNA}^{*} = 52 - j102\Omega$, consider the inductive admittance on the right of Fig. 5-15.

The admittance can be calculated as

$$Y=\frac{1}{R}+j\omega C \tag{5-11}$$

can be also presented as impedance

$$Z=\frac{1}{Y} = R//X_C \tag{5-12}$$

Including (5-11) in (5-12)

$$Z=\frac{1}{\frac{1}{R}+j\omega C} \tag{5-13}$$

then

$$Z = \frac{R - j\omega R^2 C}{(\omega RC)^2+1} \tag{5-14}$$

Hence, the complex conjugate Z_{LNA}^{*} can be represented as the phase relationship diagram on the left of Fig. 5-15 as it has the same effect of having the parallel L_{LNA} and R_{LNA} from the receiver matching network of Fig. 5-14.

Although the receiver is a differential receiver composed by the RFI_P and the RFI_N pins, the impedance matching calculation is still modeled as a single-ended port. In further sections of this chapter, the balun circuit to transform a single-ended net to a differential pair will be covered.

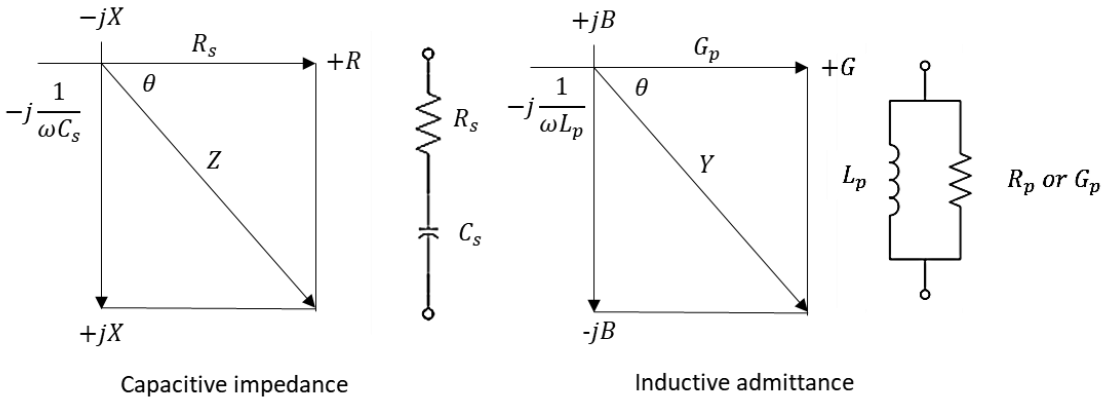

Fig. 5-15 Equivalent circuits and phase relationships. To the left, impedance with a capacitive reactance as a series connection. To the right, admittance with a capacitive susceptance as a parallel connection.

5.1.1 Receiver Impedance Matching

The impedance matching of the receiver is also based on the complex conjugate of $Z_{out}=Z_{optimal}^{*}=52 - j102\Omega$. The next step is to calculate the value of L_5, the purpose of this inductor is to shift the impedance towards the 50 Ω circle. Based on the Smit chart, the value of L_5 is around 11.64nH.

A series capacitor should shift the impedance downwards to the center of the Smith chart, as depicted in the bottom figure. The value of C_{11} is around 1.8pF.

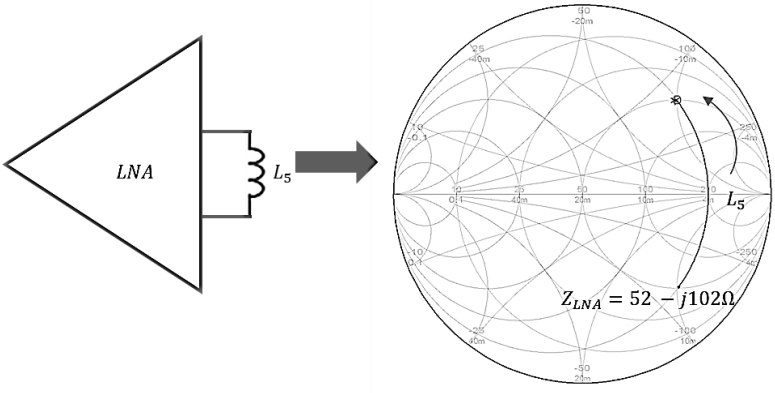

Fig. 5-16 Parallel inductor L_5 shifts impedance upwards due to inductive reactance.

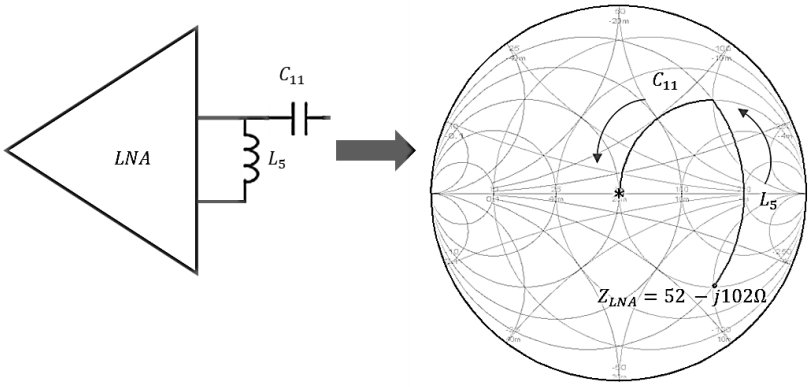

Fig. 5-17 Series capacitor C_{11} shifts impedance downwards to the center of the Smith chart. Matching the Z_{LNA} input impedance.

Being the LNA a differential low-noise amplifier, an additional circuit should be included in the receiver path to convert the signal from the antenna into a differential signal. Its analysis is covered in the next section of this chapter.

5.1.2 Balun Circuit

The antenna is a single-ended referenced to ground device. To connect it to a differential receiver, the common practice is to include a balun circuit. The balun circuit converts a balanced signal (single-ended) to an unbalanced signal (differential pair) and the other way around.

A balun with lumped components is implemented with four or six elements to ensure a voltage phase difference of 180° with equal amplitude between the lanes [1]. Fig. 5-18 represents the 50 Ω balun circuit.

The adopted balun circuit for LoRa receivers consists of only three elements. Not only this can overcome losses introduced by having a four or six elements balun because of the high value of the inductors but reduces the real state on the board. However, there is a trade-off between performance and cost.

Notice the matching network of the LNA has already been defined by the circuit composed of L_5 and C_{11} as in Fig. 5-17, adding C_{12} as the third element from the RFI_N pin to ground completes the reference balun circuit. However, the input impedance of the LNA is not infinite,

there will be a phase imbalance between RFI_P and RFI_N voltages that do not produce exactly 180° [1].

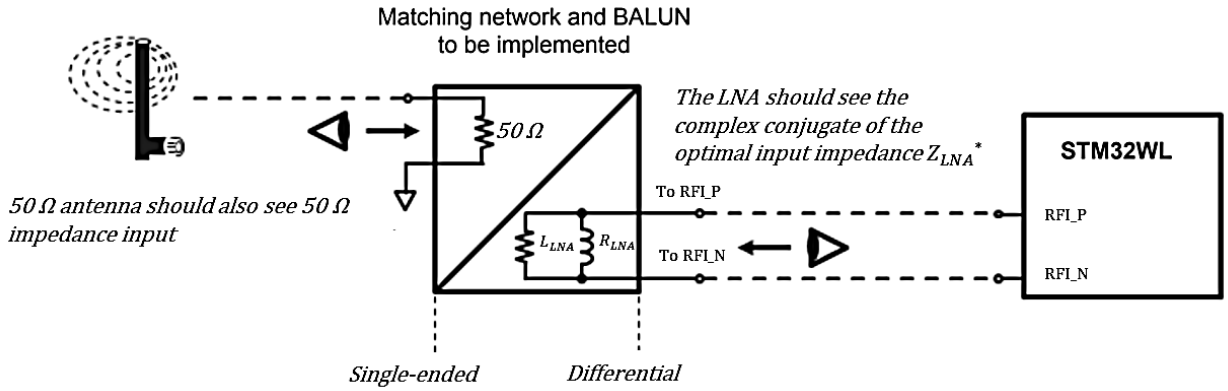

Fig. 5-18 Matching network and balun circuit representation to be implemented with lumped components on a PCB. The balun circuit transforms the single-ended signal from the antenna to a differential pair for the input receiver consisting of a differential LNA. The image is taken from [1].

The three-element balun type circuit is illustrated in Fig. 5-19.Based on the conditions that RFI_P voltage must be equal to $-RFI_N$ from [1]:

$$X_{C12}=\frac{X_{L5}}{2}, \tag{5-15}$$

The reactance of C_{12} is the half of L_5, on the other hand, L_5 is already being used to match the impedance of the LNA by canceling its reactance capacitance as seen in Fig. 5-16. Then C_{12} can be calculated as:

$$C_{12}=2\frac{\sqrt{\frac{1}{50}\left(\frac{R}{R^2+X^2}\right)-\left(\frac{R}{R^2+X^2}\right)^2}}{2\pi f}, \tag{5-16}$$

$$C_{12}=2\frac{\sqrt{\frac{1}{50}\left(\frac{52}{52^2+102^2}\right)-\left(\frac{R}{52^2+102^2}\right)^2}}{2\pi(868\text{MHz})}=2.92\text{pF}$$

Phase imbalance is always present with a three-element balun, but in practical cases is less than the simulation results as the LNA resistance is higher than the optimal resistance presented.

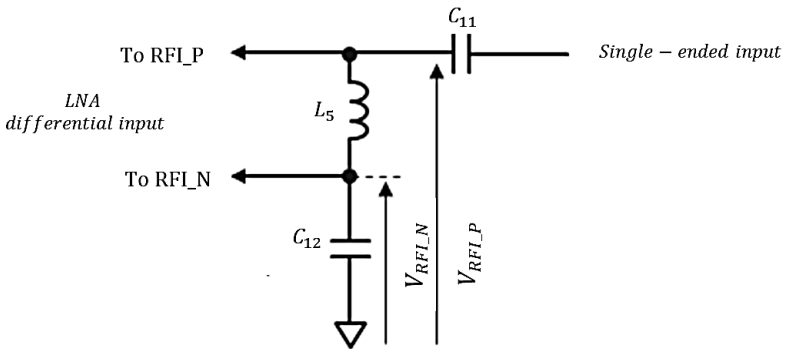

Fig. 5-19 Receiver matching network analysis. Given RFI_P=-RFI_N. The image is taken from [1].

TABLE III RECEIVER IMPEDANCE MATCHING AND FILTERING CIRCUIT VALUES OF LUMPED COMPONENTS. FIRST SEED FOR OPTIMIZATION.

PA receiver calculated values
L_5=11.64nH
C_{12}=2.92pF
C_{11}=4.85pF
C_{13}=0.7nH

The calculated values for the transmit LNA path are summarized in TABLE III. The next section presents an S-parameter analysis and transient analysis of the calculated values of the transmit and receive paths with transmission line models using ADS.

5.2. ADS circuit models.

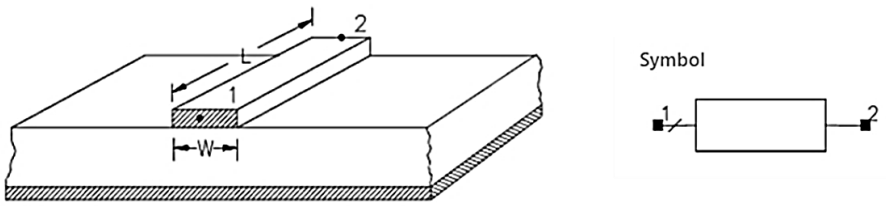

Figure 5-1 Microstrip model MLIN of ADS simulator. Range of usage $1 \leq \varepsilon_r \leq 128$ and $0.01 \leq \frac{W}{H} \leq 100$. The image is taken from [12].

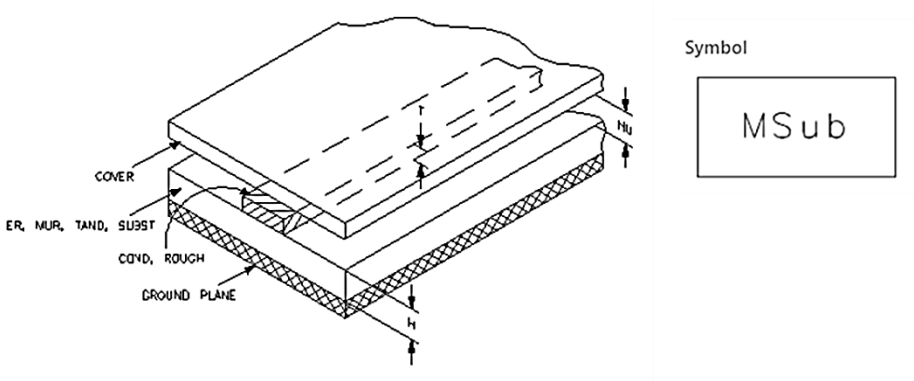

Fig. 5-20 Substrate model MSub of ADS simulator. The image is taken from [13].

The Keysight ADS simulator microstrip model used is MLIN. The ratio $\frac{W}{H} = 1.65$ and the electrical permittivity ε_r of 4.05 based on [11] stack-up makes this design suitable to use this model. Although the trace lengths are not hard-coded in the Matlab script, it was decided to fix the lengths of the traces similar to the STM32WL shield reference board [14].

The MSUB model implements *Top Layer1* as the routing layer, and *Inner Layer 2* as the reference layer from TABLE I. Considering the rest of the design parameters defined in Chapter 3, the next section describes the results of the PA transmit chain.

5.3. Transmitter Network Simulation

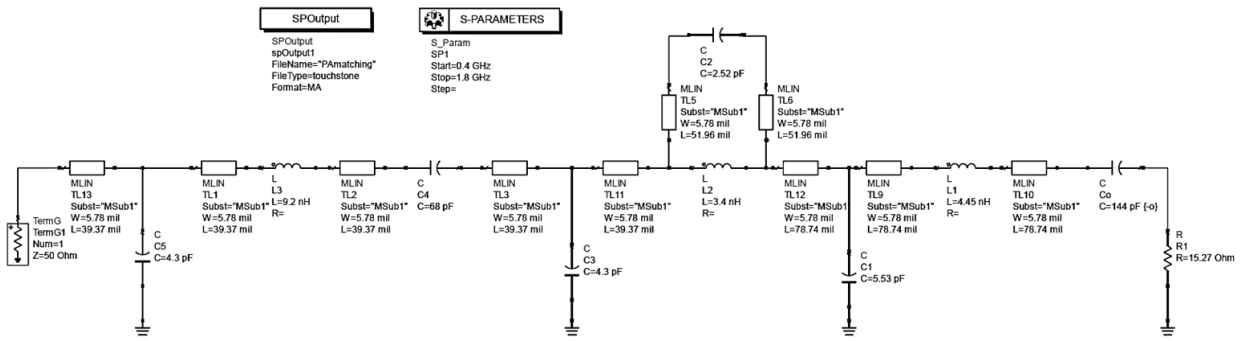

Fig. 5-21 Transmitter impedance matching and filtering network. The MLIN and MSub models are used to build the circuit in the Keysight ADS simulator. The load is the conjugate impedance of the PA optimal impedance from the load-pull analysis results.

5. MATCHING AND FILTERING NETWORKS

The circuit representing the matching and filtering network of the PA is illustrated in Fig. 5-21, the simulation results of this model and the one neglecting the effects of the transmission lines are shown in Fig. 5-22. Comparing the reflection coefficient responses from the simplified circuit (dotted line) and the one including the transmission line effects (solid line), the latter has a higher reflection coefficient close to the 868MHz with an additional coupling around 1.27GHz that could represent the H_2 harmonics effects.

Making the value C_5 the same as C_3 of the low-pass filter improves the reflection coefficient around the 868MHz band and reduces the valley near the 1.27GHz for the circuit including the MLIN and MSUB models as depicted in Fig. 5-23. The value of C_5 is used in the second seed for optimization.

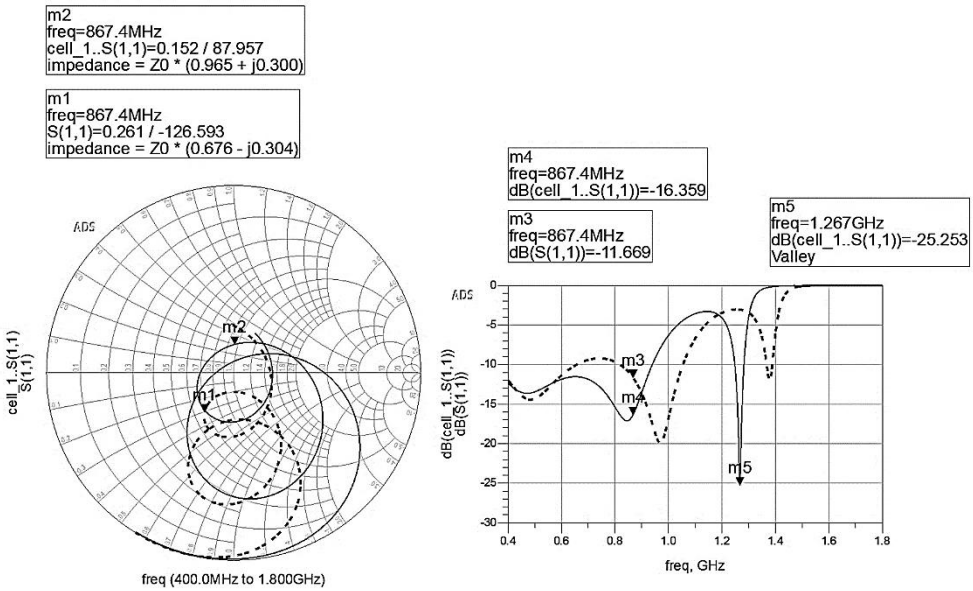

Fig. 5-22 Transmitter path. Comparison of $|S_{11}|$ of the simplified circuit (dotted line) and the circuit including MLIN and MSUB models (solid line). The dotted line $|S_{11}|$ response has greater reflections at 868MHz than the solid response.

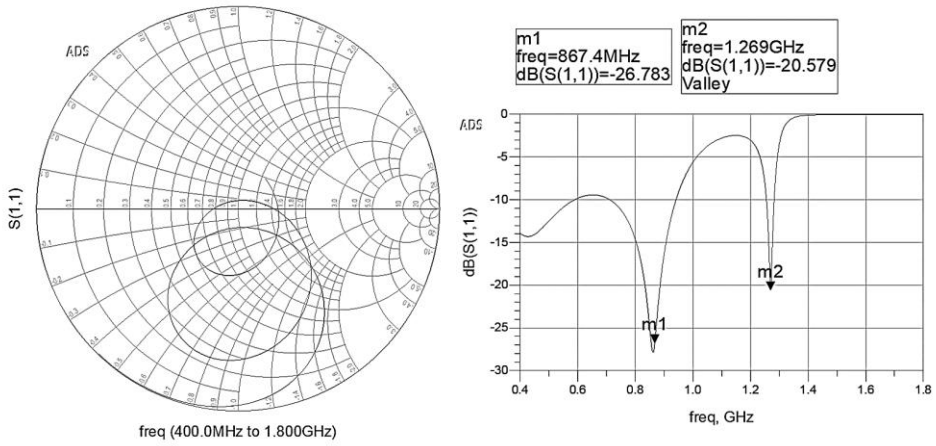

Fig. 5-23 Reflection coefficient improvement by making $C_5 = C_3$, the 1.27GHz coupling is also reduced by 5dB.

5.4. Receiver Network Simulation

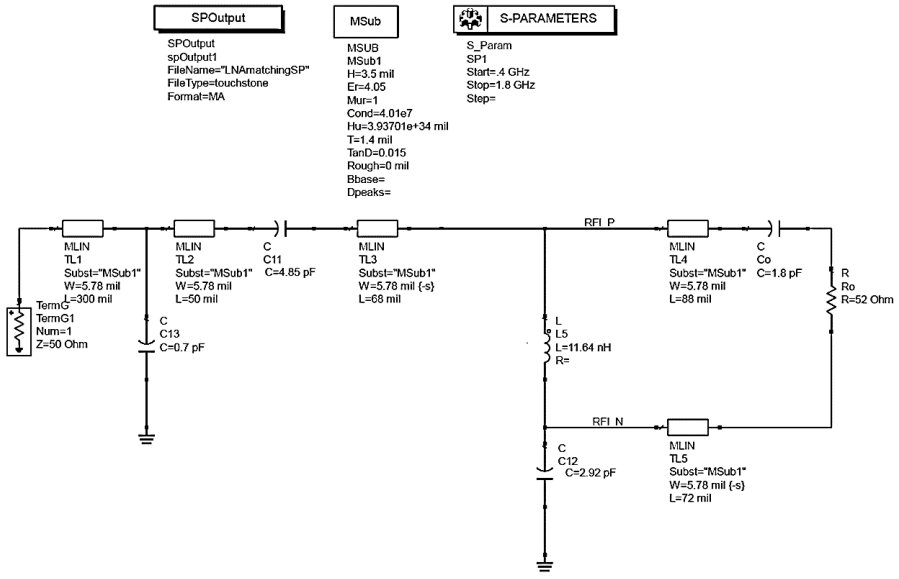

Fig. 5-24 Receiver impedance matching and filtering network. The MLIN and MSUB models are used to build the circuit in the Keysight ADS simulator. The load is the conjugate impedance of the LNA optimal impedance of the load-pull analysis results.

From the previous circuit, the same transmission line models of the PA transmitter circuit are used for the simulation. A comparison of $|S_{11}|$ responses between the circuit neglecting the transmission line effects and the one with the MLIN and MSUB models is depicted in Fig. 5-25.

To check the phase imbalance, a sine wave with 868MHz frequency is driving the LNA circuit illustrated in Fig. 5-26. The phase difference should be less in real life since the LNA resistance is usually higher than the optimal resistance.

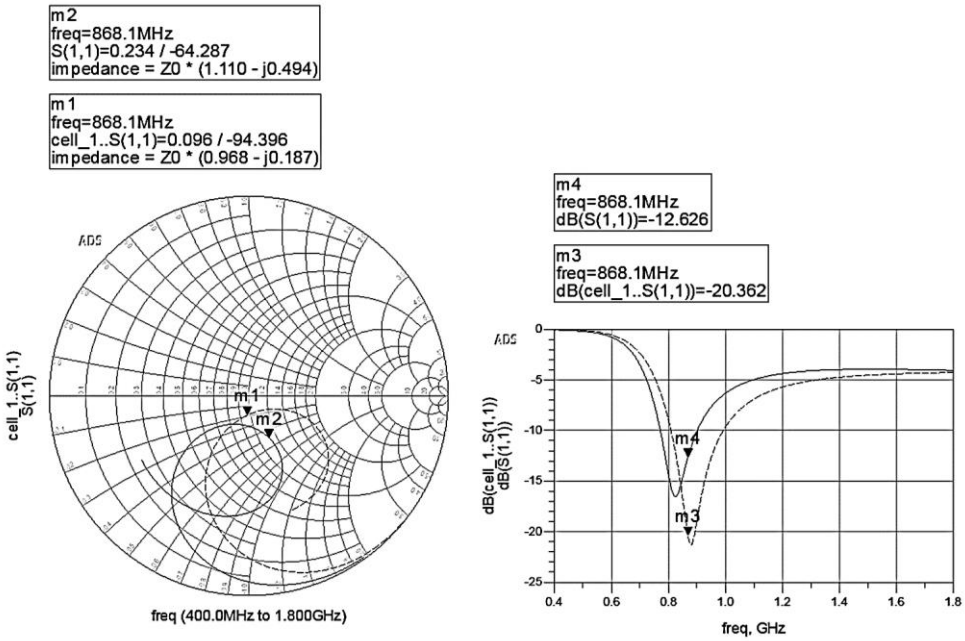

Fig. 5-25 Receiver path. Comparison of $|S_{11}|$ of the simplified circuit (dotted line) and the circuit including MLIN and MSUB models (solid line). With the transmission line model, the reflection coefficient at 868MHz increases.

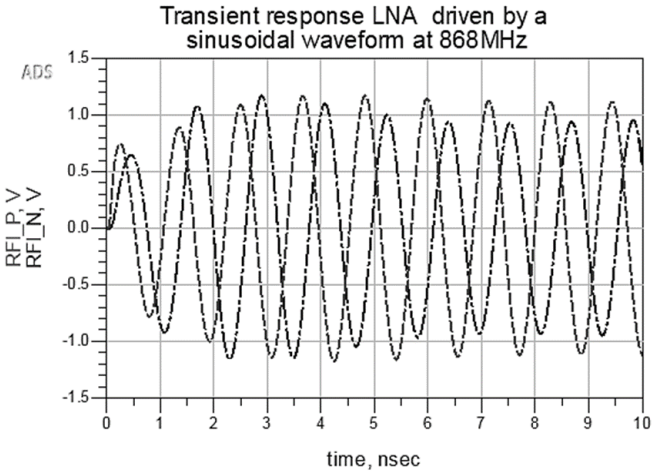

Fig. 5-26 Transient response of the LNA input after the antenna signal is transformed from a single-ended net to a differential pair. The circuit is driven by a sinusoidal waveform at 868MHz.

6. Adjusting Design Specifications

From the response of Fig. 5-22, trying to overcome the possible coupling of the harmonic filters caused by the second valley of $|S_{11}|$ around 1.3GHz, additional design specifications are included for the PA network chain. The updated specifications are as follows:

- $|S_{11}|$ > -3dB for 1.2GHz <f_0<1.6GHz
- $|S_{11}|$ > -5dB for 0.4GHz <f_0<0.7GHz
- $|S_{11}|$ < -20dB for $f_L < f_0 < f_H$ where f_L=860MHz and f_H=880MHz

On the other hand, LNA $|S_{11}|$ seems to have a better response to meet the criteria of $|S_{11}|$ < -20dB at 868MHz. However, the impact of choosing C_{12}value on the transient response phase imbalance needs to be considered. Thus, the specifications for the LNA network chain are updated:

- $|S_{11}|$ > -5dB for 1.2GHz <f_0<1.6GHz
- $|S_{11}|$ > -3dB for 0.4GHz <f_0<0.7GHz
- $|S_{11}|$ < -20dB for $f_L < f_0 < f_H$ where f_L=860MHz and f_H=880MHz
- $|RFI_P + RFI_N| < 10\%$

7. Objective Function and Optimization Parameters

This project has two optimization circuits: the PA transmitter and the LNA receiver chains. It is intended to remove the unwanted frequencies, nevertheless, due to the limitation of the circuits it is not possible to guarantee a ρ=1 outside the 868MHz, however, it is possible to improve the reflection coefficient response based on the following formulations.

The error functions are defined as a set of upper and lower boundaries. From [10]

$$e_k(\mathbf{x}) = \begin{cases} \dfrac{R_k(\mathbf{x})}{S^{ub}+\varepsilon} - 1 \text{ for all } k \in I^{ub} \\ 1 - \dfrac{R_k(\mathbf{x})}{S^{lb}+\varepsilon} \text{ for all } k \in I^{lb} \\ \dfrac{|R_k(\mathbf{x}) - S^{eq}|}{s^{ub}+\varepsilon} - 1 \text{ for all } k \in I^{eq} \end{cases} \tag{7-1}$$

$$e_k(\boldsymbol{x}) = \begin{cases} \frac{R_k(\mathbf{x})}{S^{ub}+\varepsilon} - 1 \text{ for all } k \in I^{ub} \\ 1 - \frac{R_k(\mathbf{x})}{S^{lb}+\varepsilon} \text{ for all } k \in I^{lb} \end{cases} \tag{7-2}$$

The PA transmitter response is the $|S_{11}|$ response. For the PA transmitter circuit, the following errors are identified:

- $e_1 = \frac{|S_{11}(dB)|}{S^{ub}} - 1$ for $860MHz < f_0 < 880MHz$ and $S^{ub} = -20dB$
- $e_2 = \frac{|S_{11}(dB)|}{S^{lb}} - 1$ for $400MHz < f_0 < 700MHz$ and $S^{lb} = -5dB$
- $e_3 = \frac{|S_{11}(dB)|}{S^{lb}} - 1$ for $1.2GHz < f_0 < 1.6GHz$ and $S^{lb} = -3dB$

$$e(\mathbf{x}) = [e_1 \ e_2 \ e_3]^T$$

$$\boldsymbol{\psi_{PA}} = [0.4GHz \ldots 1.6GHz]^T \text{ with } \boldsymbol{\psi_{PA}} \in \Re^{600}$$

The circuit response is presented as

$$\mathbf{R_{PA}}(\mathbf{x}) = \left|S_{11}(dB)(\mathbf{x}, \mathbf{z}, \boldsymbol{\psi}_{\mathbf{PA}})\right|$$

From the previous chapter, the LNA receiver circuit responses are $|S_{11}|$ response and phase imbalance response. For the LNA receiver circuit, the following errors are identified:

- $e_1 = \frac{|S_{11}(dB)|}{S^{ub}} - 1$ for $860MHz < f_0 < 880MHz$ and $S^{ub} = -20dB$

7. OBJECTIVE FUNCTION AND OPTIMIZATION PARAMETERS

- $e_2 = \frac{|S_{11}(dB)|}{S^{lb}}$ -1 for $400MHz < f_0 < 700MHz$ and $S^{lb} = -3dB$
- $e_3 = \frac{|S_{11}(dB)|}{S^{lb}}$ -1 for $1.2GHz < f_0 < 1.6GHz$ and $S^{lb} = -5dB$
- $e_4 = \frac{|RFI_P + RFI_N|}{S^{lb}}$ -1 with $S^{lb} = 0.1$

$$e(\boldsymbol{x}) = [\, e_1 \;\; e_2 \; e_3 \;\; e_4]^T$$
$$\boldsymbol{\psi_{LNA1}} = [0.4GHz \ldots 1.6GHz]^T \text{ with } \boldsymbol{\psi_1} \in \Re^{600}$$
$$\boldsymbol{\psi_{LNA2}} = [455ps \ldots 560ps]^T \text{ with } \boldsymbol{\psi_2} \in \Re^{300}$$

The circuit response is presented as:

$$\mathbf{R_{LNA}}(\mathbf{x}) = [|S_{11}(dB)(\mathbf{x}, \mathbf{z}, \boldsymbol{\psi}_{\mathbf{LNA1}})| \text{ Phase Imbalance}(\mathbf{x}, \mathbf{z}, \boldsymbol{\psi}_{\mathbf{LNA2}})].$$

8. Optimization Results

For the gradient-based methods, the following parameters were considered:

- Gradient step size h $= 1\text{x}10^{-2}$
- Function tolerance ε_g=1x10^{-3}
- Optimization variables tolerance ε_x=1x10^{-2}
- Maximum number of iterations 100
- Line search boundaries $\alpha^{\text{lb}} = 0.01$

For the Nelder-Mead method:

- Function tolerance ε_g=1x10^{-3}
- Optimization variables tolerance ε_x=1x10^{-2}
- Maximum number of iterations 100

Optimization variables are normalized and limited by box constraints transformation unless specified.

8.1. Transmitter Optimization

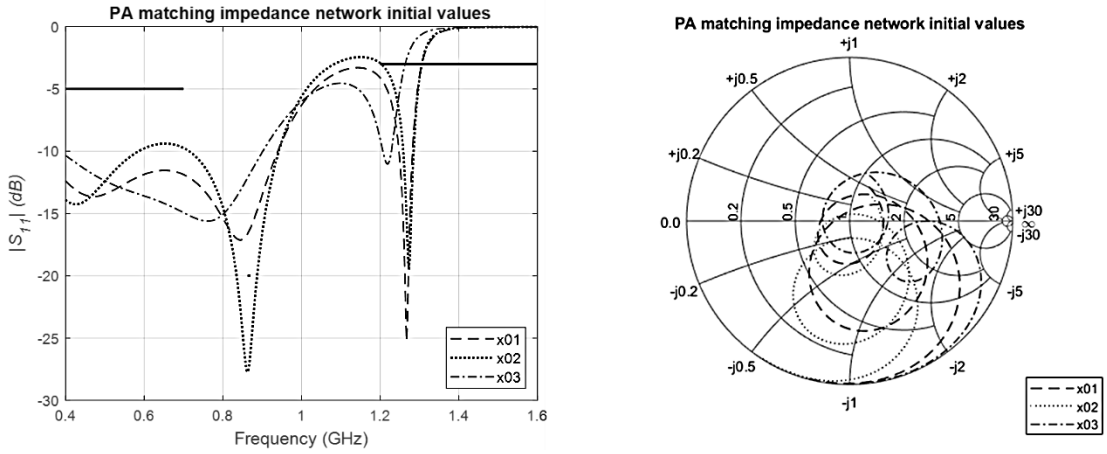

Fig. 8-1 Transmitter path $|S_{11}|$ response of the three starting points.

The seeds used during the optimization process for the transmit chain are the following:

- $\mathbf{x_{01}}^{\text{T}} = [4.45 \quad 5.53 \quad 2.52 \quad 3.4 \quad 4.3 \quad 9.2 \quad 3.5]$
- $\mathbf{x_{02}}^{\text{T}} = [4.45 \quad 5.5 \quad 2.5 \quad 3.4 \quad 4.3 \quad 9.2 \quad 4.3]$

8. OPTIMIZATION RESULTS

- $\mathbf{x_{03}}^T = [4.5 \quad 5 \quad 2.7 \quad 3.5 \quad 4.7 \quad 9.2 \quad 2.7]$

The results of the initial points are illustrated Fig. 8-1. The first approach was to test the feasibility of the optimization algorithms to meet the required goals without any boundaries. Fig. 8-2 illustrates the Conjugate Gradient reduction of the error function within 38 iterations with the first seed. The final negative value of the error function indicates the optimization goals are met. It can also be seen the value of the inductor L_3 nearly doubled its size and C_1 was reduced significantly. Based on the previous, it was easier to define box constraints aiming to assist the optimization methods in finding a solution. The box constraints applied were $x^{lb}=[\ 4\ \ 2\ \ 2\ \ 4\ \ 3\ \ 15\ \ 2\ ]^T$ and $x^{lb}=[\ 5\ \ 3\ \ 3\ \ 6\ \ 4\ \ 18\ \ 4\ ]^T$.

Comparing the Conjugate Gradient optimization results of the first seed without constraints as shown in TABLE IV and the results in TABLE V where the aforementioned limits were applied, both performances meet the optimization goals, however, the latter yields much faster after only 6 iterations compared to the 38 iterations of the unbounded optimization variables. The reflection coefficient of both optimization results is depicted in Fig. 8-3 and Fig. 8-4.

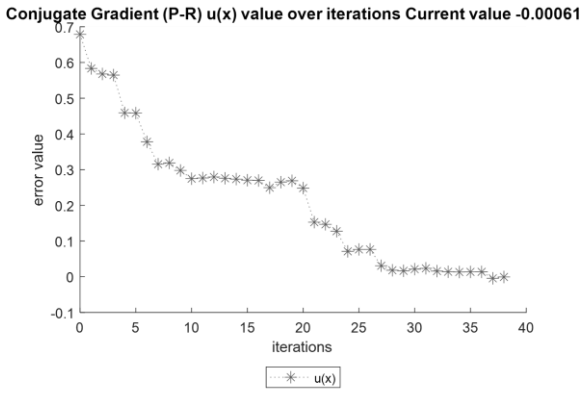

Fig. 8-2 Error function value after 38 iterations using the first seed. The error value over iterations is obtained with the Conjugate Gradient method with the Polak-Ribiére formula. The negative final value indicates the optimization goals were met.

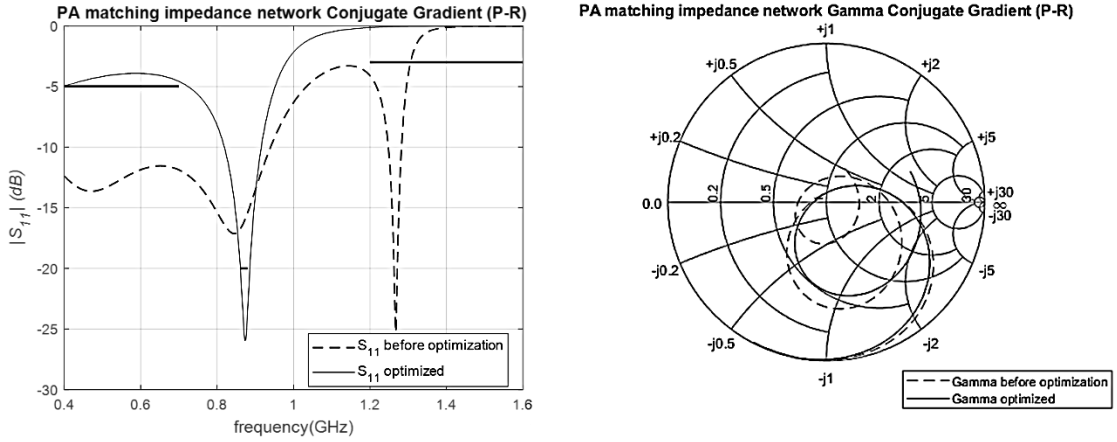

Fig. 8-3 Conjugate-Gradient using Polak-Ribiére formula optimization of $|S_{11}|$ response. First seed, no box constraints, 38 iterations, 1362 function evaluations. Stopping criteria u(**x**) small enough. Transmitter.

TABLE IV
OPTIMIZATION RESULTS SCALED NON-CONSTRAINED OPTIMIZATION VARIABLES USING CONJUGATE GRADIENT. FIRST SEED. TRANSMITTER

$\mathbf{x}_0^{*T}$	**Method**	**Formula**	$\mathbf{x}^{*T}$	$u(\mathbf{x}^*)$	Iter	OFE	EF
[4.45 5.53 2.52 3.4 4.3 9.2 3.5] First seed	Conjugate Gradient	P-R	[4.59 1.43 2.61 4.57 3.74 16.9 3.43]	-0.0006	38	1362	2

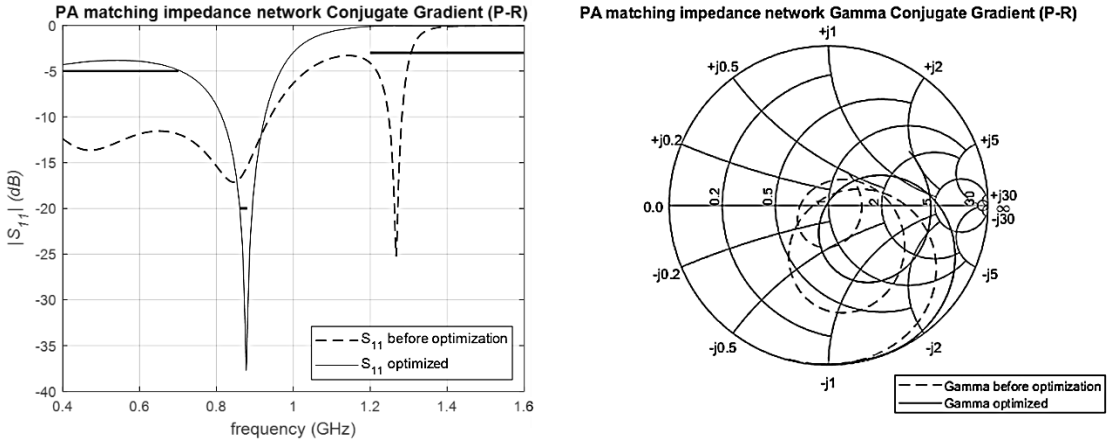

Fig. 8-4 Conjugate-Gradient Polak-Ribiére formula optimization of $|S_{11}|$ response. First seed, $x_{lb} = [\,4\ \ 2\ \ 2\ \ 4\ \ 3\ \ 15\ \ 2\,]^T$ and $x_{ub} = [\,5\ \ 3\ \ 3\ \ 6\ \ 4\ \ 18\ \ 4\,]^T$. 6 iterations, 227 function evaluations. Stopping criteria u(**x**) small enough Transmitter.

TABLE V
OPTIMIZATION RESULTS WITH SCALED OPTIMIZATION VARIABLES AND APPLYING BOX CONSTRAINTS USING CONJUGATE GRADIENT. FIRST SEED. TRANSMITTER

x_0^{*T}	Method	x_{lb}^T x_{ub}^T	x^{*T}	$u(x^*)$	Iter	OFE	EF
[4.45 5.53 2.52 3.4 4.3 9.2 3.5] First seed	Conjugate Gradient (P-R)	[4 2 2 4 3 15 2] [5 3 3 6 4 18 4]	[4.02 2.17 2.8 4.89 3.27 18 2.48]	-0.01229	6	227	2

8.1.1 Transmitter Optimization Same Box Constraints

The following table compares the results of the different optimization methods applied to the three seeds with the same set of box constraints. Reflection coefficient responses before and after optimization are illustrated after this table in Fig. 8-5 and Fig. 8-6.

Conjugate Gradient and Quasi-Newton methods applied to optimize the second seed yield very similar optimization results after only 5 iterations. A comparison of the normalized optimization variables change over iterations between these two methods is shown in Fig. 8-7.

The Nelder-Mead method reaches the maximum iteration limit in the attempt to optimize the third seed, the reason for this is the escape criteria considering both $TolX \leq \varepsilon_x$ and $TolFun \leq \varepsilon_g$ parameters to be satisfied, in contrast with the implemented gradient-based methods where the error function sign is also monitored reducing the number of iterations. This can be observed in Fig. 8-8 where the Conjugate Gradient and Nelder-Mead error functions are compared after the optimization. The latter took 8 iterations compared to Nelder-Mead reaching the maximum number of iterations after the optimization of the third seed.

TABLE VI
OPTIMIZATION RESULTS. NORMALIZING OPTIMIZATION VARIABLES AND APPLYING THE SAME BOX CONSTRAINTS. TRANSMITTER

$\mathbf{x}_0^{*T}$	**Method**	$x_{lb}^T\ x_{ub}^T$	$\mathbf{x}^{*T}$	$u(\mathbf{x}^*)$	Iter	OFE	EF
[4.45 5.53 2.52 3.4 4.3 9.2 3.5] First seed	Nelder-Mead	[4 2 2 4 3 15 2] [5 3 3 6 4 18 4]	[4.06 2.12 2.8 5.05 3.21 18 2.21]^T	-0.0136	100	173	0
[4.45 5.53 2.52 3.4 4.3 9.2 3.5] First seed	Conjugate Gradient (P-R)	[4 2 2 4 3 15 2] [5 3 3 6 4 18 4]	[4.02 2.17 2.8 4.89 3.27 18 2.48]	-0.0123	6	227	2
[4.45 5.53 2.52 3.4 4.3 9.2 3.5] First seed	Quasi-Newton (BFGS)	[4 2 2 4 3 15 2] [5 3 3 6 4 18 4]	[4.03 2.53 2.92 5.31 3.28 17.9 3.2]	-0.0589	9	235	2
[4.45 5.5 2.5 3.4 4.3 9.2 4.3] Second seed	Nelder-Mead	[4 2 2 4 3 15 2] [5 3 3 6 4 18 4]	[4 2.43 2.83 5.21 3.07 18 2.02]^T	-0.006	100	170	0
[4.45 5.5 2.5 3.4 4.3 9.2 4.3] Second seed	Conjugate Gradient (P-R)	[4 2 2 4 3 15 2] [5 3 3 6 4 18 4]	[4.02 2.12 2.8 4.83 3.2 18 2.05]	-0.0057	5	198	2
[4.45 5.5 2.5 3.4 4.3 9.2 4.3] Second seed	Quasi-Newton (BFGS)	[4 2 2 4 3 15 2] [5 3 3 6 4 18 4]	[4.02 2.19 2.81 4.93 3.16 18 2.02]	-0.0058	5	121	2
[4.2 5 2.7 3.5 4.7 9.2 2.7] Third seed	Nelder-Mead	[4 2 2 4 3 15 2] [5 3 3 6 4 18 4]	[4.57 2.28 2.83 5.24 3.13 17.9 2.78]^T	-0.0417	100	159	0

8. OPTIMIZATION RESULTS

[4.2 5 2.7 3.5 4.7 9.2 2.7] Third seed	Conjugate Gradient (P-R)	[4 2 2 4 3 15 2] [5 3 3 6 4 18 4]	[4.47 2.52 2.77 5.32 3 17.8 2.29]	-0.0021	8	319	2
[4.2 5 2.7 3.5 4.7 9.2 2.7] Third seed	Quasi-Newton (SR1)	[4 2 2 4 3 15 2] [5 3 3 6 4 18 4]	[4.26 2.41 2.93 5.2 3.03 18 2.05]	-0.0025	27	589	2

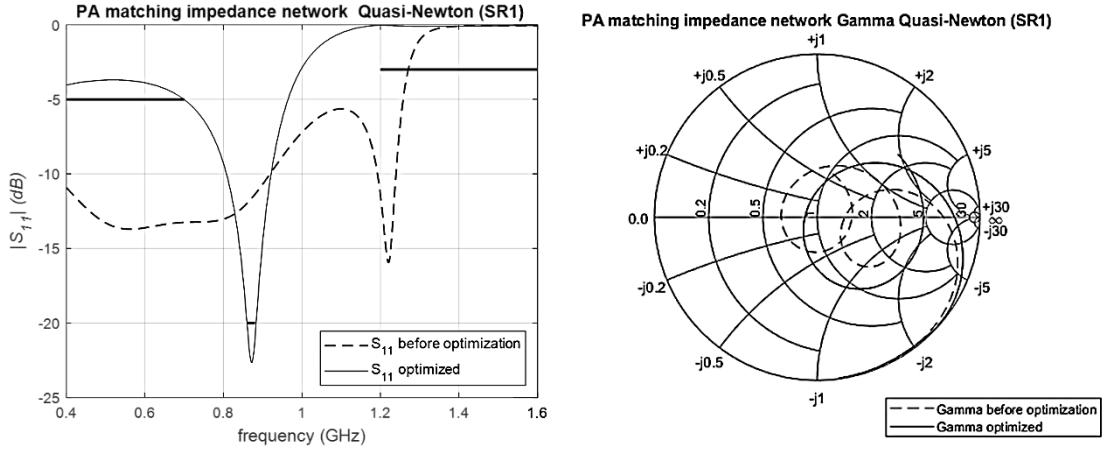

Fig. 8-5 Quasi-Newton Symmetric-Rank-One formula optimization of $|S_{11}|$ response. Third seed, 27 iterations, 589 function evaluations. Stopping criteria u(**x**) small enough. Box constraints $x_{lb} = [\,4\ \ 2\ \ 2\ \ 4\ \ 3\ \ 15\ \ 2\,]^T$ and $x_{ub} = [\,5\ \ 3\ \ 3\ \ 6\ \ 4\ \ 18\ \ 4\,]^T$. Transmitter.

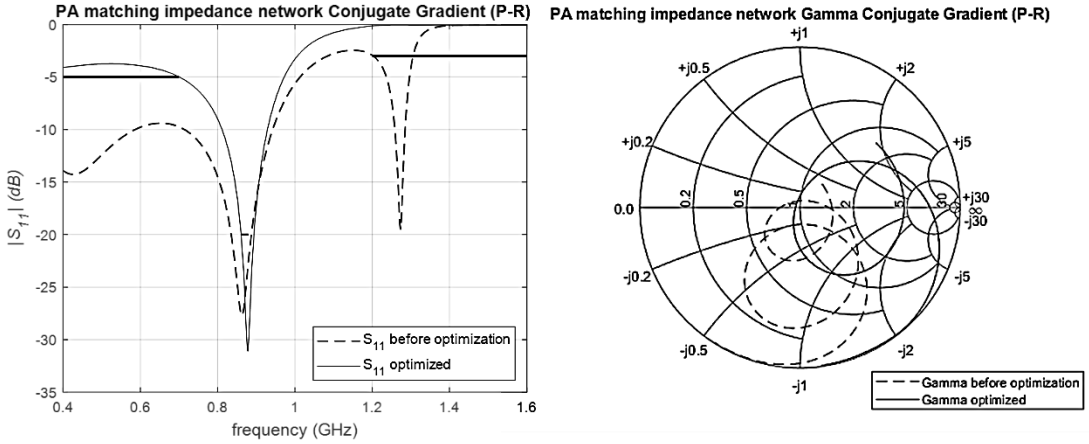

Fig. 8-6 Conjugate Gradient Polak-Ribiére formula optimization of $|S_{11}|$ response. Second seed, 5 iterations, 198 function evaluations. Stopping criteria u(**x**) small enough. Box constraints $x_{lb} = [\,4\ \ 2\ \ 2\ \ 4\ \ 3\ \ 15\ \ 2\,]^T$ and $x_{ub} = [\,5\ \ 3\ \ 3\ \ 6\ \ 4\ \ 18\ \ 4\,]^T$. Transmitter.

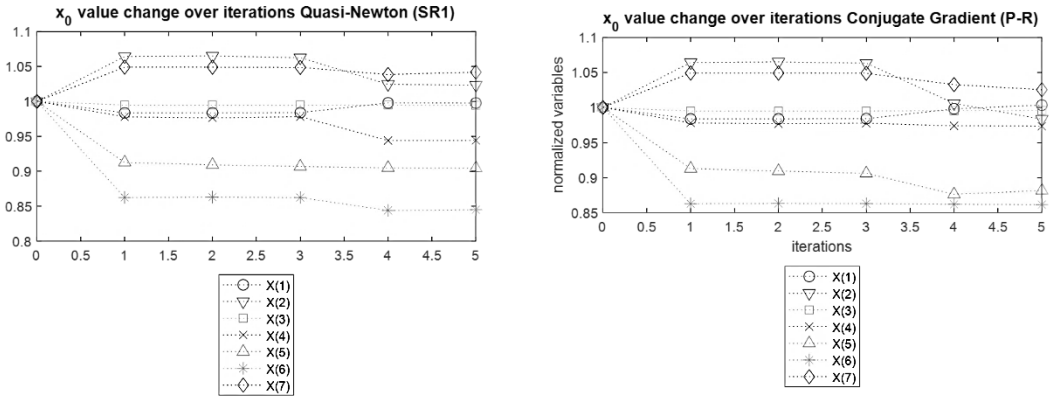

Fig. 8-7 Quasi-Newton SR1 formula and Conjugate Gradient P-R formula change of normalized optimization variables. Second seed, box constraints $x_{lb} = [\,4\ \ 2\ \ 2\ \ 4\ \ 3\ 15\ \ 2\,]^{T}$ and $x_{ub} = [\,5\ \ 3\ \ 3\ \ 6\ \ 4\ \ 18\ \ 4\,]^{T}$. Transmitter. The same number of iterations and a similar pattern.

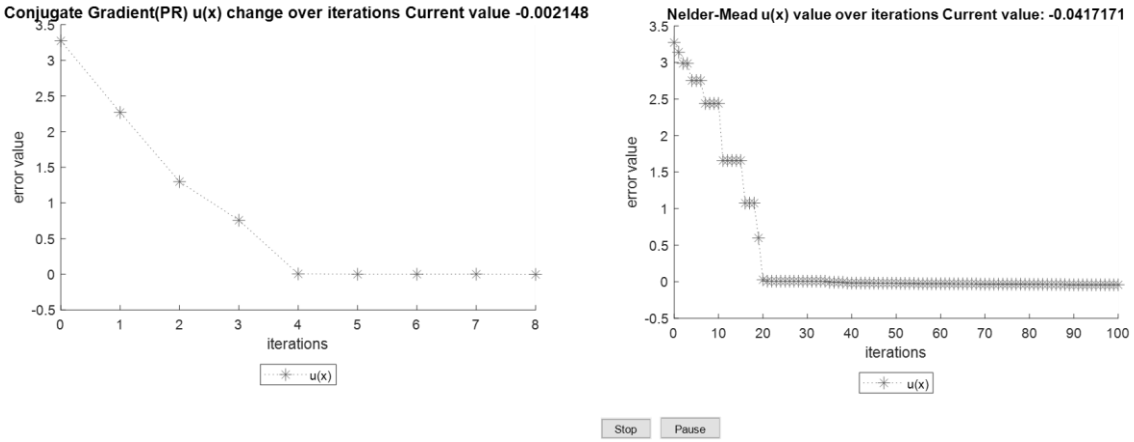

Fig. 8-8 Conjugate Gradient Polak-Ribiére formula and Nelder-Mead error function over iterations. Third seed, box constraints $x_{lb} = [\,4\ \ 2\ \ 2\ \ 4\ \ 3\ 15\ \ 2\,]^{T}$ and $x_{ub} = [\,5\ \ 3\ \ 3\ \ 6\ \ 4\ \ 18\ \ 4\,]^{T}$. Transmitter. Conjugate Gradient yields a faster response than Nelder-Mead.

8.2. Receiver Optimization

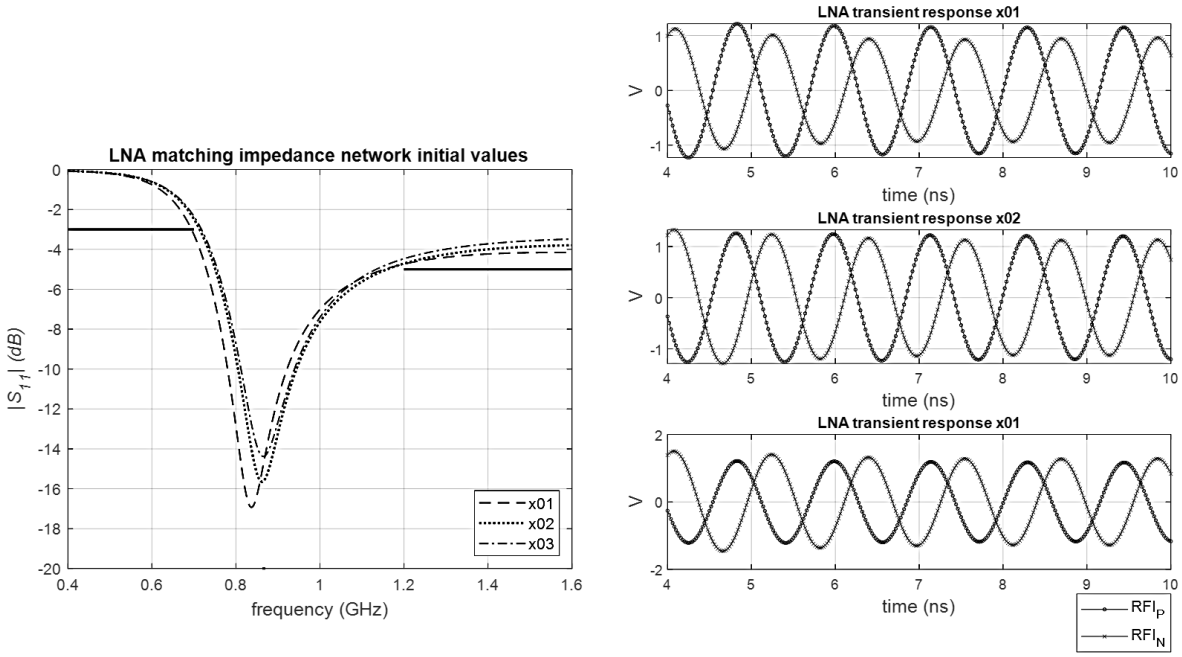

Fig. 8-9 Receiver path $|S_{11}|$ and balun transient responses of the three starting points.

The following initial values are set to optimize the LNA path. The first seed is obtained from Chapter 4.

- $\mathbf{x_{01}}^T = [4.85 \quad 11.64 \quad 2.92 \quad 0.7]$
- $\mathbf{x_{02}}^T = [5 \quad 11 \quad 3 \quad 1]$
- $\mathbf{x_{03}}^T = [6 \quad 11 \quad 2.7 \quad 1.2]$

Given the initial $|S_{11}|$ responses of the LNA happen to be near to the optimization goals as shown in Fig. 8-9, the box constraints were chosen close to the seed values. Still, including the phase imbalance goal of the transient response limits the improvement of the reflection coefficient as large changes on the balun circuit elements are limited to avoid it.

The box constraints are set as $x^{lb}=[5 \ 10 \ 2 \ 0.5]^T$ and $x^{ub}=[8 \ 11 \ 3.5 \ 1.5]^T$. As an initial approach, Conjugate Gradient with the Polak-Ribiére formula is employed for all seeds- The results are presented in the next figures and tables.

The reflection coefficient response after optimization is very similar between the second and third seeds as illustrated in Fig. 8-11 and Fig. 8-12, however, the second seed is better for the

Conjugate Gradient algorithm due to the reduction of the number of iterations compared to the first and third seeds.

TABLE VII
FIRST SEED OPTIMIZATION RESULTS. NORMALIZING OPTIMIZATION VARIABLES AND APPLYING BOX CONSTRAINTS USING ONLY CONJUGATE GRADIENT. RECEIVER

$\mathbf{x}_0^{*T}$	**Method**	x_{lb}^T x_{ub}^T	$\mathbf{x}^{*T}$	$u(\mathbf{x}^*)$	Iter	OFE	EF	Reference Figure
[4.85 11.64 2.92 0.7] First seed	Conjugate Gradient (P-R)	[5 10 2 0.5] [8 11 3.5 1.5]	[6.43 10.5 3.5 1.3]	-0.0047	8	207	2	Fig. 8-10
[5 11 3 1] Second seed	Conjugate Gradient (P-R)	[5 10 2 0.5] [7 12 4 2]	[6.43 10.4 3.49 1.35]	-0.0073	13	294	2	Fig. 8-11
[6 11 2.7 1.2] Third seed	Conjugate Gradient (P-R)	[5 10 2 0.5] [7 12 4 2]	[7.46 10.3 3.5 1.45]	-.0123	8	203	2	Fig. 8-12

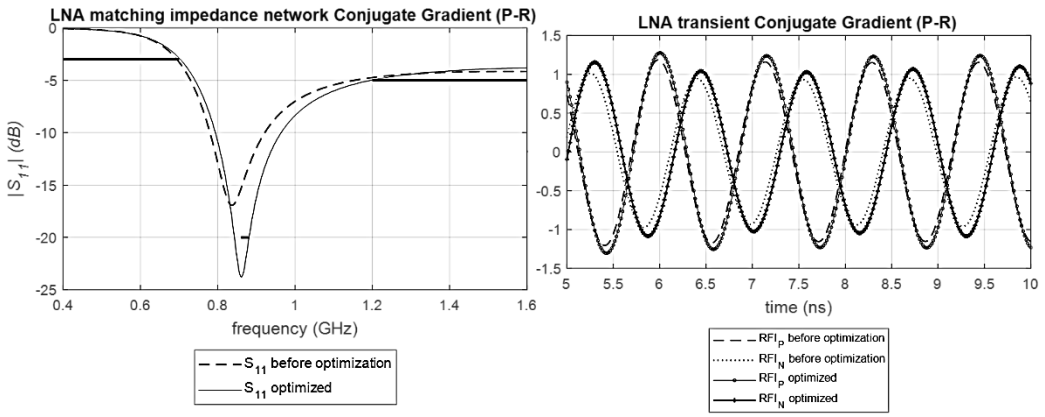

Fig. 8-10 Conjugate Gradient using Polak-Ribiére formula optimization of $|S_{11}|$ and transient response. First seed, box constraints $x_{lb}^T = [\ 5\ \ 10\ \ 2\ \ 0.5\ ]$ and $x_{ub}^T = [\ 8\ \ 11\ \ 3.5\ \ 1.5\ ]$. 8 iterations, 207 function evaluations. Stopping criteria $u(\mathbf{x})$ small enough.

8. OPTIMIZATION RESULTS

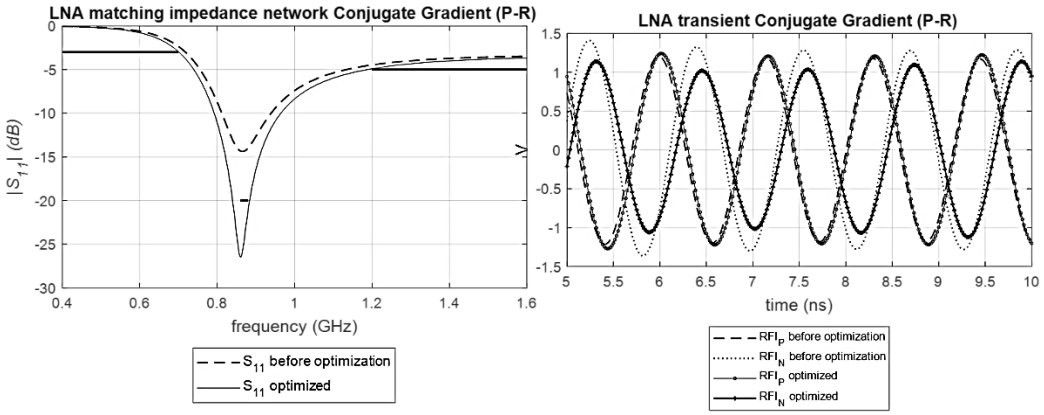

Fig. 8-11 Conjugate Gradient using Polak-Ribiére formula optimization of $|S_{11}|$ and transient response. Second seed, box constraints $x_{lb}{}^{T} = [\ 5\ \ 10\ \ 2\ \ 0.5\ ]$ and $x_{ub}{}^{T} = [\ 8\ \ 11\ \ 3.5\ \ 1.5\ ]$. 13 iterations, 294 function evaluations. Stopping criteria u(**x**) small enough.

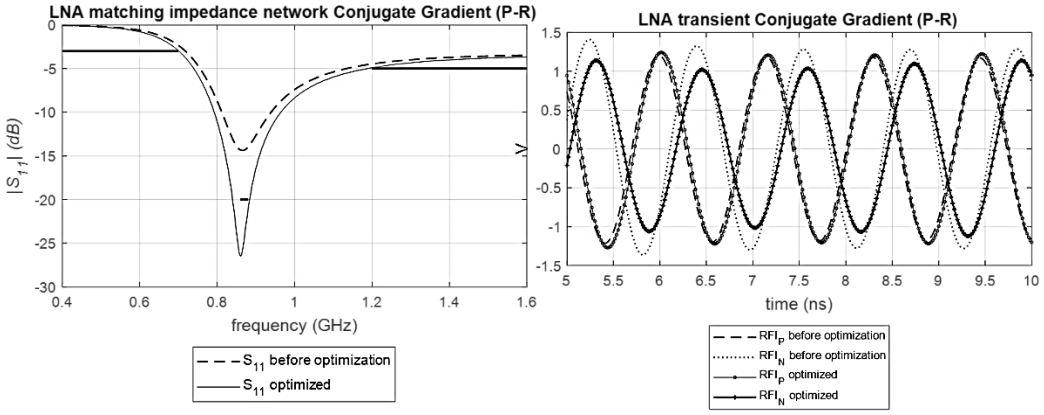

Fig. 8-12 Conjugate Gradient using Polak-Ribiére formula optimization of $|S_{11}|$ and transient response. Third seed, box constraints $x_{lb}{}^{T} = [\ 5\ \ 10\ \ 2\ \ 0.5\ ]$ and $x_{ub}{}^{T} = [\ 8\ \ 11\ \ 3.5\ \ 1.5\ ]$. 8 iterations, 203 function evaluations. Stopping criteria u(**x**) small enough.

The third seed and same box constraints were implemented with Quasi-Newton and Nelder-Mead yielding a very similar reflection coefficient and transient responses as shown in Fig. 8-13 and **Error! Reference source not found.**. Moreover, Quasi-Newton finds a solution in only 6 iterations compared to 68 from the Nelder-Mead algorithm as depicted in **Error! Reference source not found.**.

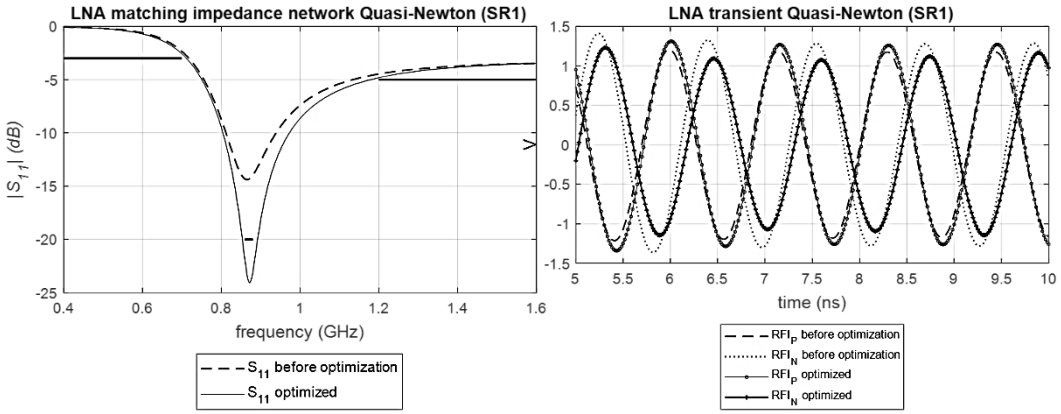

Fig. 8-13 Quasi-Newton using Symmetric-Rank-One formula optimization of $|S_{11}|$ and transient response. Third seed, box constraints $x_{lb}{}^{T} = [\ 5\ \ 10\ \ 2\ \ 0.5\ ]$ and $x_{ub}{}^{T} = [\ 7\ \ 12\ \ 4\ \ 2\ ]$. 6 iterations, 112 function evaluations. Stopping criteria u(**x**) small enough.

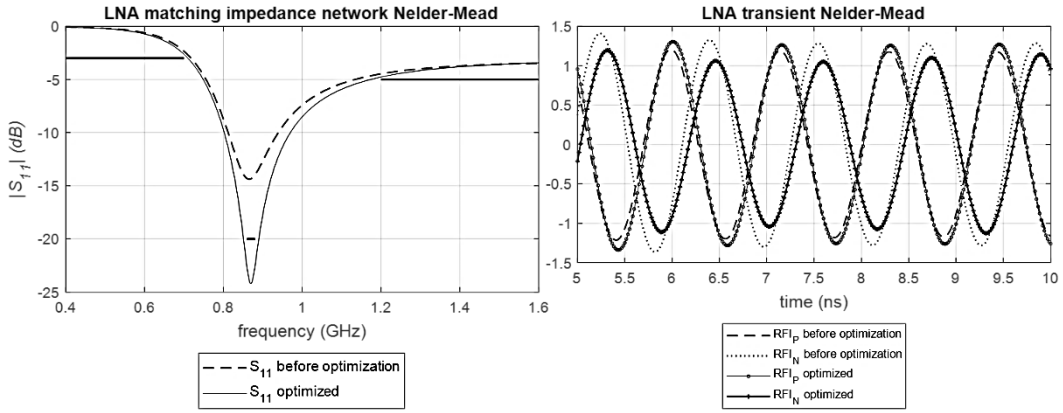

Fig. 8-14 Nelder-Mead optimizations of $|S_{11}|$ and transient response. Third seed, box constraints $x_{lb}{}^{T} = [\ 5\ \ 10\ \ 2\ \ 0.5\ ]$ and $x_{ub}{}^{T} = [\ 7\ \ 12\ \ 4\ \ 2\ ]$. 68 iterations, 120 function evaluations. Stopping criteria u(**x**) and **x** relative change small enough.

8. OPTIMIZATION RESULTS

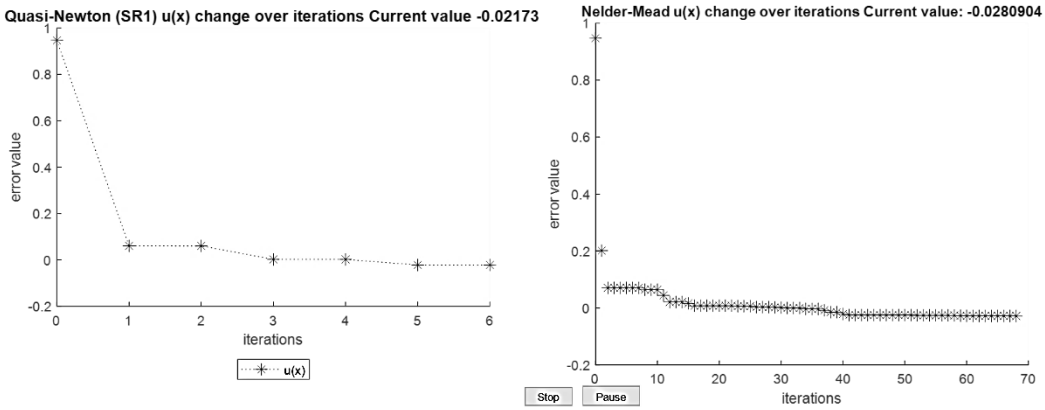

Fig. 8-15 Quasi-Newton SR1 formula and Nelder-Mead error function over iterations. Third seed, box constraints $x_{lb}{}^{T} = [\ 5\ \ 10\ \ 2\ \ 0.5\ ]$ and $x_{ub}{}^{T} = [\ 7\ \ 12\ \ 4\ \ 2\ ]$. Transmitter. Quasi-Newton took more iterations, but the error is smaller compared to Conjugate Gradient.

TABLE VIII depicts the Quasi-Newton and Nelder-Mead results with the previous box constraints.

TABLE VIII
OPTIMIZATION RESULTS. NORMALIZING OPTIMIZATION VARIABLES AND APPLYING THE SAME BOX CONSTRAINTS AS CONJUGATE GRADIENT. RECEIVER

$\mathbf{x}_0{}^{*T}$	**Method**	$x_{lb}{}^{T}\ x_{ub}{}^{T}$	$\mathbf{x}^{*T}$	$u(\mathbf{x}^{*})$	Iter	OFE	EF
[4.85 11.64 2.92 0.7] First seed	Nelder-Mead	[5 10 2 0.5] [8 11 3.5 1.5]-	[6.73 10.5 3.34 1.3]	-0.0050	75	131	1
[4.85 11.64 2.92 0.7] First seed	Conjugate Gradient	[5 10 2 0.5] [8 11 3.5 1.5]-	[6.43 10.5 3.5 1.3]	-0.0047	8	207	2
[4.85 11.64 2.92 0.7] First seed	Quasi-Newton (SR1)	[5 10 2 0.5] [8 11 3.5 1.5]-	[7.13 10.4 3.43 1.42]	-0.0129	9	164	2
[5 11 3 1] Second seed	Nelder-Mead	[5 10 2 0.5] [8 11 3.5 1.5]-	[6.75 10.3 3.5 1.41]	-0.0125	57	105	1
[5 11 3 1] Second seed	Conjugate Gradient	[5 10 2 0.5] [8 11 3.5 1.5]-	[6.43 10.4 3.49 1.35]	-0.0073	13	294	2
[5 11 3 1] Second seed	Quasi-Newton (BFGS)	[5 10 2 0.5] [8 11 3.5 1.5]-	[6.28 10.5 3.5 1.28]	-0.0040	5	98	2
[6 11 2.7 1.2] Third seed	Nelder-Mead	[5 10 2 0.5] [8 11 3.5 1.5]-	[7.02 10.2 3.5 1.48]	-0.0169	43	79	1

[6 11 2.7 1.2] Third seed	Conjugate Gradient	[5 10 2 0.5] [8 11 3.5 1.5]-	[7.46 10.3 3.5 1.45]	-0.0124	8	203	2
[6 11 2.7 1.2] Third seed	Quasi-Newton (SR1)	[5 10 2 0.5] [8 11 3.5 1.5]-	[7.49 10.3 3.5 1.47]	-0.0149	6	127	2

8.2.1 Receiver Optimization with Different Box Constraints

From the findings, it appears the box constraints can overcome the values of the seeds. To test this idea, different sets of box constraints are applied.

The following table depicts different sets of implemented optimization parameters, followed by some figures comparing the results of the optimization methods for some of the seeds.

TABLE IX
OPTIMIZATION RESULTS. NORMALIZING OPTIMIZATION VARIABLES AND APPLYING DIFFERENT BOX CONSTRAINTS. RECEIVER

$\mathbf{x}_0^{*T}$	**Method**	x_{lb}^T x_{ub}^T	$\mathbf{x}^{*T}$	$u(\mathbf{x}^*)$	Iter	OFE	EF
[4.85 11.64 2.92 0.7] First seed	Nelder-Mead	[4 9 2 1] [7 12 4 2]	[7 9.81 3.99 1.78]	-0.0205	84	152	1
[4.85 11.64 2.92 0.7] First seed	Quasi-Newton (BFGS)	[5 9 3 1] [8 11 4 2]	[5.97 10.2 3.65 1.44]	-0.0038	36	493	2
[6 11 2.7 1.2] Third seed	Conjugate Gradient (P-R)	[7 9 3 1] [8 11 4 2]	[7.27 9.78 3.97 1.97]	-0.0117	4	110	2
[5 11 3 1] Second seed	Quasi-Newton (BFGS)	[5 8 2 1] [8 11 4 2]	[6.29 9.86 3.97 1.6]	-0.0030	52	686	2
[6 11 2.7 1.2] Third seed	Nelder-Mead	[6 9 3 1] [8 12 4 2]	[7.98 9.78 3.96 1.95]	-0.0395	49	92	1

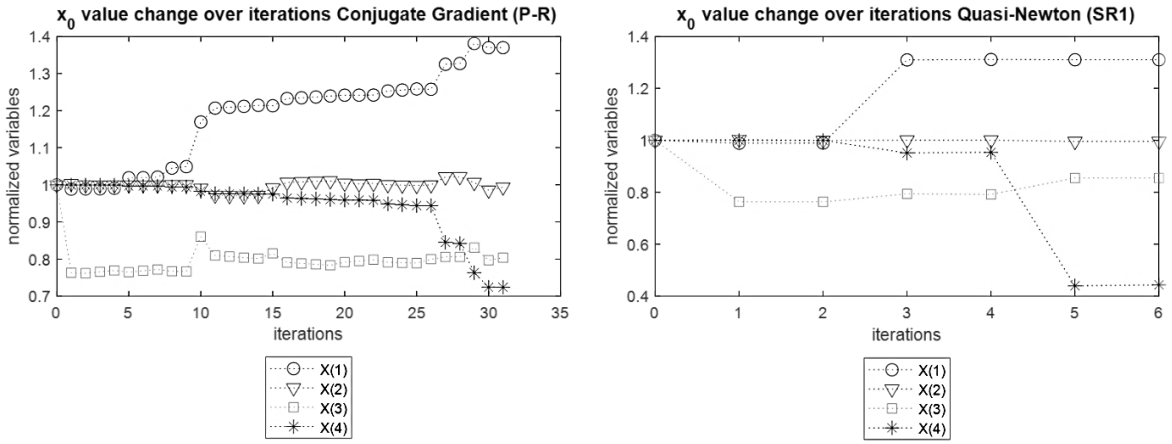

Fig. 8-16 Conjugate Gradient P-R formula and Quasi-Newton SR1 formula optimization variables change over iterations. Third seed, box constraints x_{lb}^T= [5 10 2 0.5] and x_{ub}^T = [7 12 4 2]. Transmitter. The variables have a similar pattern, but Quasi-Newton yields faster.

8.3. Optimization Results Remarks

The optimization space set by the box constraints compensates for the unsatisfactory initial responses of the seeds as seen in the previous results.

On the other hand, from the results shown in TABLE IX, if the optimization space is wide, the gradient-based algorithms will take longer to converge. This can be observed with the second seed after applying Quasi-Newton with new box constraints the optimization was done after 52 iterations compared to applying the boundaries from TABLE VIII where the same seed was optimized after only 5 iterations with the same method.

Changing the limits for the third seed improved the Conjugate Gradient method as the optimization changed from 31 iterations with the previous box constraints to only 4 iterations.

Applying limits to the optimization variables with the different optimization algorithms yields very similar circuit responses meeting the optimization goals; however, the limits must be relatively close to the minimum solution of the objective function to obtain a faster response, even worse incorrect boundaries can yield the algorithms to diverge.

Regarding the implemented gradient-based algorithms and the computational cost, the maximum number of function evaluations representing simulator callbacks was obtained by optimizing the PA transmitter circuit without boundaries resulting in 1362 function evaluations.

Making use of a workstation with an Intel(R) Core (TM) i7-3820QM CPU @ 2.70GHz with 32GB RAM the optimization time for the aforementioned was around 18 minutes.

An additional observation is the number of function evaluations performed during the screening process to bound the exact line search; these are quantified together with the function evaluations while minimizing the objective function, in either case, the number of simulator callbacks is related to the number of the optimization variables for each iteration. One could assume the transmitter should have a significantly higher number of simulator callbacks compared to the receiver circuit due to the larger number of optimization variables, however, the latter is restricted by the complexity of the objective function since it also considers the transient response of the differential receiver additional to the reflection coefficient.

Although it is not presented in this essay, the number of points of the independent variable n in $\boldsymbol{\psi} \in \mathfrak{R}^{n}$, also influence the convergence for this optimization case study, as more points inside the range of interest create a higher workload for the optimization algorithms while attempting to minimize the maximum error. A trade-off should be considered with the number of frequency or time points and the outcome of the optimization results, as selecting a small number of points could be insufficient to generate the desired circuit optimizable response.

Conclusions and Future Work

Impedance matching is a complex task since any disturbance in the values of the lumped components or even irregularities on PCB stack-up and traces due to manufacturing capabilities greatly impact the reflection coefficient. However, it is also a common industry practice to follow suppliers' impedance matching guidelines to achieve maximum performance. Moreover, including simulations during the design process to identify discrepancies in the circuit response before prototyping is essential. An example has been reported in Chapter 4 regarding the initial values of the PA stage, where after optimizing, the final values differed greatly from the initial ones.

An advantage of having a digital control on the transmitter (STM32WL) for the PA output is the configuration of the output power. Optimal settings can be configured to set the output power, this should also be considered as part of the optimization-dependent variables. In contrast, the LNA receiver phase imbalance is always present when applying a three-element balun, it is proportional to the resistance of the LNA, being higher in practical cases as mentioned in [1], with a higher load the phase imbalance is reduced, hence it should be measured. With this information, a better phase imbalance error could be formulated.

Although this work presented a theoretical approach to maintain a minimum reflection coefficient on the transmitter and receiver sides, it cannot substitute the design verification with real laboratory equipment, particularly the PA stage, where more controls are frequently implemented to comply with regulatory agencies across the globe. It's important to mention that the updated goals presented in Chapter 5 have not been certified with any regulatory agency, but it is of great interest to test the circuit capabilities and tune the reflection coefficient response based on optimization results, to reduce hefty verification cycles in the final mandatory certification process.

A good practice to reduce computational cost when optimizing a circuit is limiting the number of optimization variables, this can be done by fixing some components values, however for this design, where different impedance matching and filtering stages co-exist, it was left to the optimization algorithms to improve the necessary values to meet the goals, this can be seen in the

results section where some optimized values resemble the initial ones. Furthermore, these components can be identified by the experienced RF designer.

From all the above, for any circuit optimization study is crucial to have a suitable circuit model and a well-defined objective function, the exerted could be lacking to include models of real components based on the supplier's S-parameter files together with some variations to the nominal values. In contrast, the implemented gradient-based algorithms in Matlab had good responses when applying box constraints to the optimization variables suggesting non-ideal elements could be included to create a better-founded model.

Although the implemented line search methods do not guarantee an absolute minimum, for this case study of circuit optimization it is not required due to the design space and lumped components range, it is better to rely on the box constraints not only to limit the optimization space but to make sure the final component values are within a suitable range to outsource the Bill of Materials.

In addition, the Matlab scripts can be easily tailored to drive other simulators that do not require exhausting computational effort. Likewise, this analysis is valid for any LoRa transceiver application, regardless of the vendor if the PA and LNA load-pull analysis data is available together with a defined PCB stack-up.

Related to future work, implementing the design based on the stack-up presented in Chapter 3 will imply modifying the transmission line widths of the current model; however, using the same parametric file it can be updated. With this information, a new set of optimization variables can be found. Furthermore, it would be of interest to compare the performance of the transceiver by verifying the actual impact on the output power with the optimized results. Also, this project could be a candidate to implement space mapping techniques by using the current setup as a coarse model and replacing the fine simulation model with actual measurements of the output power and transient responses from the PCB together with more realistic models such as IBIS.

To finalize, for this RF impedance matching and filtering case study, it can be confirmed the implemented gradient-based algorithms with Matlab scripts can converge with good results even if the seed is not close to the optimal solution as long as the box constraints are tight and close to the minimum solution. Then again, for more reliable results one must create a well-structured objective function.

Bibliography

[Banarjee-02] A. Banerjee, *Automated Broad and Narrow Band Impedance Matching for RF and Microwave Circuits*, Springer, 2019.

[Choma-03] J. Choma."Scattering Parameters Concept Theory Applications" [Online], Nov 2002. Available: https://www.ieee.li/pdf/essay/scattering_parameters_concept_theory_applications.pdf.

[Del-Rey-05] J. R. Del Rey, "Circuit Optimization Performed on High Frequency Structures by Applying Classical Optimization Techniques", MEng. dissertation, Dept. Elect. Eng., ITESO Univ., Tlaaquepaque, Jal., 2012.

[Jiménez-González-08] M. A. Jiménez-González, "Self-Cascode OTA design and optimization using classical optimization methods," Dept. Elect. Eng., ITESO Univ., Tlaaquepaque, Jal., 2021.

[JLCPCB-11] JLCPCB. (2021). *Impedance matching stack-up* [Online]. Available: https://cart.jlcpcb.com/impedance.

[Keysight-12] Keysight Technologies. (2008). *ADS Distributed Components - Microstrip Components - MLIN* [Online]. Available: https://edadocs.software.keysight.com/pages/viewpage.action?pageId=6264361.

[Keysight-13] Keysight Technologies, *ADS Distributed Components - Microstrip Components - MSUB* [Online]. Available: https://edadocs.software.keysight.com/pages/viewpage.action?pageId=5912136.

[Rayas-Sánchez-04] J. E. Rayas-Sánchez, "Box Constraints-Restricting Optimization Space," [Online]. Available https://desi.iteso.mx/erayas/documents/CirOpt_course/Lectures/Optimization/Opt_Constrained_methods.pdf.

[Rayas-Sánchez-06] J. E. Rayas-Sánchez, "Optimization Unconstrained Methods," [Online]. Available: https://desi.iteso.mx/erayas/documents/CirOpt_course/Lectures/Optimization/Opt_Unconstrained_methods.pdf.

[Rayas-Sánchez-07] J. Rayas-Sánchez, "Optimization Unidimensional methods," [Online]. Available: https://desi.iteso.mx/erayas/documents/CirOpt_course/Lectures/Optimization/Opt_Unidimensional_methods.pdf.

[Rayas-Sánchez-09] J. E. Rayas-Sánchez, "A General Formulation to Nominal Design Optimization," [Online]. Available: https://desi.iteso.mx/erayas/documents/CirOpt_course/Lectures/Cir_Opt_PE/Circuit_Opt.pdf.

[Rayas-Sánchez-10] J. E. Rayas-Sánchez, "Minimax Formulation to Design Optimization," [Online]. Available: https://desi.iteso.mx/erayas/documents/CirOpt_course/Lectures/Cir_Opt_PE/Circuit_Opt.pdf.

[STMicro-01] STMicroelectronics, "AN5457 RF matching network design guide for STM32WL Series", 2020.

[STMicro-14] STMicroelectronics, "STM32WL Reference Board MB1720 XO IO Shield," [Online]. Available: 2020. https://www.st.com/resource/en/hw_model/stm32wl_reference_board_mb1720-xo_ios_shield.7z.